

TOPICAL REVIEW • OPEN ACCESS

# Printed and flexible organic and inorganic memristor devices for non-volatile memory applications

To cite this article: Ayoub H Jaafar *et al* 2023 *J. Phys. D: Appl. Phys.* **56** 503002

View the [article online](#) for updates and enhancements.

You may also like

- [Scalable and Green Fabrication of Thin-Film Solar Cells Using Solution Processed Inkjet Printing Method](#)  
Poonam Sundriyal and Shantanu Bhattacharya
- [Promising applications of graphene and graphene-based nanostructures](#)  
Bich Ha Nguyen and Van Hieu Nguyen
- [Capacity Enhancement of Low-Cost and Flexible Micro-Supercapacitors By a Redox-Active Electrolyte and Laser-Induced Fibrous Graphene](#)  
Aamir Minhas-Khan and Gerd Grau

## Topical Review

# Printed and flexible organic and inorganic memristor devices for non-volatile memory applications

Ayoub H Jaafar<sup>1</sup> , Alex Gee<sup>2</sup>  and N T Kemp<sup>1,\*</sup> <sup>1</sup> School of Physics and Astronomy, University of Nottingham, Nottingham NG7 2RD, United Kingdom<sup>2</sup> Department of Materials, University of Oxford, Oxford OX1 3PH, United KingdomE-mail: [Neil.Kemp@nottingham.ac.uk](mailto:Neil.Kemp@nottingham.ac.uk)

Received 28 March 2023, revised 4 July 2023

Accepted for publication 18 September 2023

Published 28 September 2023



CrossMark

## Abstract

The electronics market is highly competitive and driven by consumers desire for the latest and most sophisticated devices at the lowest cost. In the last decade there has been increasing interest in printing electronic materials on lightweight and flexible substrates such as plastics and fabrics. This not only lowers fabrication and capital costs but also facilitates many new applications, such as flexible displays and wearable electronics. The printing of computer memory is also desirable since many of these applications require memory to store and process information. In addition, there is now an international effort to develop new types of computer memory that consume ultra-low levels of power. This is not only to lower energy usage worldwide, which is important for reducing CO<sub>2</sub> emissions, but it also enables a longer period between the re-charging of devices such as mobile phones, music players and fitness bands. Memory that is non-volatile is an obvious choice since it does not consume power to retain information like conventional SRAM and DRAM. Memristors (or memory resistor) are a new type of memory that are intrinsically non-volatile in nature. Their simple two-terminal architecture, easy method of fabrication and low power consumption means they have received much attention from both the research community and industry. Devices with the lowest fabrication costs are made from organic or hybrid (organic–inorganic) composite materials because of the ability to use low-cost solution processing methods with the advantages of large area deposition under vacuum-free and room temperature ambient conditions. Memristors have excellent device properties, including a large resistance Off/On ratio (up to 5 orders of magnitude), fast switching speeds (less than 15 ns), long endurance (over 10<sup>12</sup> cycles), long data storage retention time (~10 years) and high scalability down to nanoscale dimensions. In this article we review progress in the field of printed and flexible memristor devices and discuss their potential across a wide range of applications.

\* Author to whom any correspondence should be addressed.



Original content from this work may be used under the terms of the [Creative Commons Attribution 4.0 licence](https://creativecommons.org/licenses/by/4.0/). Any further distribution of this work must maintain attribution to the author(s) and the title of the work, journal citation and DOI.

Keywords: printed memristors, resistive memory, RRAM, solution processing, hybrid material, flexible, review

(Some figures may appear in colour only in the online journal)

## 1. Introduction

In the last several decades, organic and hybrid (organic–inorganic) composite materials have received enormous attention worldwide because of the wide range of new applications for printed electronics on flexible and lightweight substrates. There is increasing demand for electronic devices that can be used in a variety of non-conventional environments and applications, which traditionally would not be considered appropriate for fragile and expensive semiconductor devices that are susceptible to easy breakage or damage from the elements. A typical example is in wearable technologies where there are substantial new market opportunities for electronics that can be embedded in clothing and sportswear. Applications also include diagnostic health monitoring of the wearer, embedded sensors for chemical sensing in hazardous environments, electronic clothing and prosthetics that are dynamically adjustable or can change their material properties depending on the temperature, humidity and needs of the wearer. Printed electronics applications are also numerous and include electronic displays, security tags, sensors, solar cells, flexible batteries, electronic skin (e-skin) and flexible printed circuit boards, see figure 1. Since many of these applications also require computer memory for data storage, processing and device operation, there is also a need for having memory devices that can be deposited on flexible and lightweight substrates. Next generation non-volatile memories are an obvious choice, since non-volatile memory has the benefit of not requiring energy to retain information, which is important for many applications such as wearable and portable electronic devices, where it is important to maximise the time between battery re-charging.

Another important aspect of developing new types of computer memory is the increasing need for new types of computing architectures. Since the 1960's computing power and memory technologies have been driven by Moore's Law, which is a relationship that describes how the density of transistor components per unit area doubles every 18 months [1, 2]. However, Moore's Law is coming to an end since it is increasingly more and more difficult to reduce the transistor size whilst retaining adequate device properties [3]. Thus, the world is beginning to witness a new era of computing that is likely to be driven by new unconventional methods of computing and post-von-Neumann architectures such as neuromorphic and in-memory computing [4–6]. This will likely also involve new types of memory devices that have both a very small footprint and ultra-low energy usage [7]. Memristors (or memory resistor) are a new type of memory that are intrinsically non-volatile in nature [8, 9].

Memristors have enormous advantages because of their two-terminal architecture, ultra-low power, simple fabrication, low-cost manufacture, suitability for synaptic computing and their capacity for ultra-high density data storage. In recent years, memristor performances have advanced considerably. Very high levels of endurance (120 billion cycles) and retention (>10 years) have been achieved, and ultra-high-density crossbar arrays have been realized [10] with scalability down  $\sim 2$  nm. Whilst, much initial research has focussed on metal-oxides for the active switching material, memristors based on organics and hybrid materials have also come of age, with new device types having high performance levels such as very large Off/On resistance ratios (up to  $10^5$  orders of magnitude [11]), fast switching speeds (less than 15 ns, see [12]), long endurance (over  $10^{12}$  cycles [13]), and long data storage retention time ( $\sim 10$  years [14]), low-cost fabrication on rigid and flexible substrates [15] as well as high density integration and demonstrated potential in neuromorphic computing [16].

Printed electronic fabrication techniques offer several potentially significant advantages including low cost, fast processing and scalable fabrication of micro and nano-patterning on lightweight, portable, curved, and flexible substrates [17–19]. Already, there are extremely promising research level examples that demonstrate the appealing aspects of these devices. One of these is a fully printed molybdenum disulfide ( $\text{MoS}_2$ ) memristor crossbar device reported by Feng *et al* [20]. The Ag/ $\text{MoS}_2$ /Ag device printed on a flexible polyimide substrate, see figure 2, exhibited both volatile and non-volatile switching properties (controllable via the compliance current) that successfully emulated both the short-term and long-term synaptic plasticity of biological synapses. The printed devices also exhibited a large resistance Off/On ratio (up to  $10^7$ ), a low switching voltage (0.18 V), and ultra-low power consumption (1 fW). Another fully printed crossbar memristor array has been demonstrated by Catenacci *et al* [21]. In this case, the device was made from a nano-composite material of Cu-SiO<sub>2</sub> nanowires embedded in ethylcellulose and printed between Cu and Au electrodes. The devices showed reliable switching (up to  $10^4$  cycles) and had write speeds as fast as 3  $\mu\text{s}$  with retention times of  $10^6$  s. Altogether, these results along with other recently observed interesting electrical and optical phenomena [22, 23] indicate high promise for the use of these low-dimensional 1D and 2D materials in a range of energy efficient neuromorphic computing applications.

The following sections review progress in this exciting area of new memory technologies based on memristors. The focus is on the field of organic and hybrid (organic–inorganic) composite materials since these offer new opportunities for applications that require flexible substrates and/or manufacture by

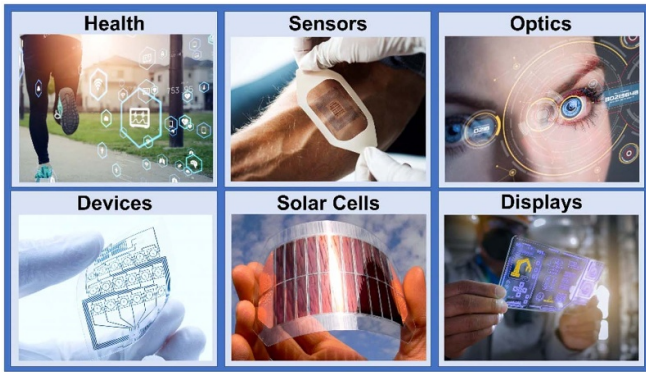


**Figure 1.** A wide range of applications for printed electronics on flexible and lightweight substrates. iStock.com/metamorworks/Rawpixel/shawn\_hempel/LYagovy/Darika Dasopa.

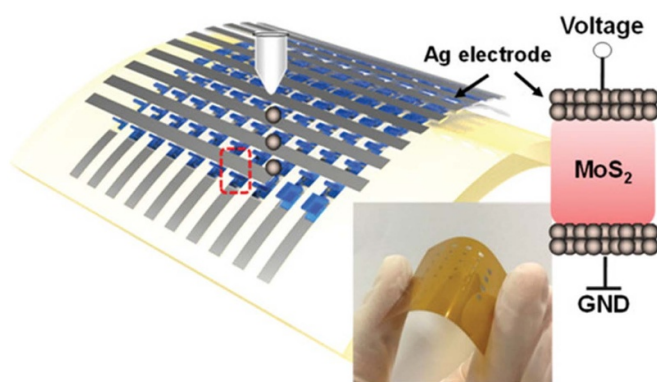


**Figure 2.** Fully printed Ag/MoS<sub>2</sub>/Ag crossbar memristor on flexible polyimide substrate. Reproduced from [20]. CC BY 4.0.

low-cost, printed technologies. The current state of the art will be presented along with a discussion of memristor device properties, switching mechanisms and their potential for use in a flexible and printed electronics.

## 2. Memristor operation principles

Before discussing organic and hybrid materials based memristors it is worth briefly to describe the operation of a conventional memristor. Memristors or resistive random-access memory devices operate as memory devices due to the possibility to switch their resistance between a high resistance state (HRS) and a low resistance state (LRS) via application of an external stimulus. Both resistance states are stable at  $V = 0$ , which means that memristors can be used as a non-volatile memory. The switching from a HRS to a LRS is called a SET process, whereas, the switching from a LRS to a HRS is called a RESET process. Resistive switching phenomenon can be classified into bipolar and unipolar types depending upon the polarity of the applied potential required for switching. The occurrence of SET and RESET processes at different polarity is referred to as bipolar resistive switching. In the case of unipolar switching, SET and RESET processes occur at the same polarity but with different magnitudes of the applied stimulus.

Many memristor types, including both metal oxides [24] and organic based memristors [25], require an electrical forming process to initiate switching in devices. This typically involves applying a high potential to form defects or conductive filaments within the material which then provide reliable resistive switching at a much lower potential. Upon forming, a compliance current is applied to prevent irreversible damage and runaway breakdown processes that can occur due to the high current passing through device. Forming processes are generally considered as being undesirable as it requires an extra step in the fabrication process. Also, since the properties of forming are highly stochastic in nature and the current-voltage properties are highly non-linear, it can introduce large variability between devices. At present, there are increasingly more non-forming device types being reported. Many of these function because of a large number of intrinsic defects, as in the case of oxide-based devices [26], or a high concentration of loading traps, such as that mediated by metal nanoparticles (NPs) as in hybrid organic–inorganic devices [14].

From the fabrication point of view, memristors based on inorganic materials such as oxides are often fabricated *via* techniques such as sputtering, atomic layer deposition, metal evaporation and chemical and physical vapor deposition [27–32]. These techniques require expensive equipment and the processes involved are not well-suited for high-throughput fabrication. For example, sputtering, atomic layer deposition and metal evaporation must all be done under high vacuum conditions which is a slow process since it takes considerable time to remove air from the vacuum chamber. Additionally, the processes involve high temperatures that are not compatible with the use of soft materials such as those needed for flexible substrates. In contrast, organic or hybrid organic–inorganic materials-based memristors can be fabricated *via* solution processing techniques such as spin-coating, dip coating, drop casting and printing technologies like ink-jet printing, 3D printing and screen printing. They also offer advantages of low cost, vacuum-free conditions, fast deposition times and large area fabrication on lightweight and flexible substrates under ambient conditions [15, 33–37].

The key parameters used to compare device types across research and industry, which also governs their compatibility for different applications are endurance and retention. Endurance can be defined as the maximum number of write/erase or SET/RESET cycles that a device can achieve before it becomes unreliable or deviates outside the allowed operation resistance Off/On window. Retention is defined as the capability of a device to retain its resistance state over a period of time. For reliable non-volatile memory applications, resistive switching devices should have at least endurance cycles and retention time of  $10^6$ – $10^7$  cycles and  $>10$  years, respectively [38].

Memristors have several potential applications. The most obvious being non-volatile random-access memory. Here, one of the main advantages is that unlike current SRAM and DRAM technologies, memristors do not require continuous power to retain data [39] and therefore large energy savings can be made. This is particularly relevant today because of global warming, high electricity costs because of the global

energy crisis and the recent surge in new A.I. technologies, such as ChatGPT and AlphaGo, which consume enormous amounts of energy for their training. Since memristors are only 2-terminal devices, they also have the advantage of a smaller footprint compared to 3-terminal (transistor-type) devices, which means a greater packing of data on a chip and overall, more computing power. The writing of data for memory storage is also a faster and simpler process and is achieved by the application of a voltage pulse that switches the device between either its HRS or LRS, corresponding to either a 0 bit or a 1 bit. The stored data can as well be easily retrieved by applying a low voltage pulse to read its resistance.

Memristors also have enormous potential for use in neuromorphic computing systems [40] since they have properties that directly emulate the analogue switching and learning characteristics of biological synapses. This makes them promising candidates for a whole range of artificial intelligence applications such as combined memory/computational elements for in-memory computing, synaptic sensors for vision [41] and image recognition [42], and ultra-low computing architectures for edge-computing and large-scale neuromorphic computing systems [43].

Another significant application of memristors is in logic circuits integrated with CMOS chips. As a memory element, crossbar memristors can be fabricated directly on the CMOS and used as the reconfigurable data routing network [44], and logic-in-memory applications [45].

Organic and hybrid material based memristors can be classified into four main categories based on their structure, these are the following:

- i. Single layer structure consisting of one organic/polymer layer sandwiched between top and bottom metal contacts.
- ii. Bi-layer structure consisting of two different organic/polymer layers sandwiched between top and bottom metal contacts.
- iii. Tri-layer structure consisting of metal/semiconductor nano-traps dispersed in a thin film that is deposited between two organic/polymer layers and sandwiched between top and bottom metal contacts.
- iv. Single layer structure consisting of a hybrid organic–inorganic material (often a nanocomposite) that is sandwiched between top and bottom metal contacts.

This article focusses on the simplest memristor architecture which consists of only a single active layer (categories I and IV) and examines their switching properties and switching mechanisms. The following two sections focus on single layer memristor devices made from organic and hybrid (organic–inorganic) composite materials.

### 3. Single layer organic memristors

Organic electronic memristors containing a single layer (thin-film) of a resistive switching material are fabricated by depositing the active layer between top and bottom metal electrodes in a vertical sandwich-like structure as shown schematically in figure 3. Materials that can be used include small organic

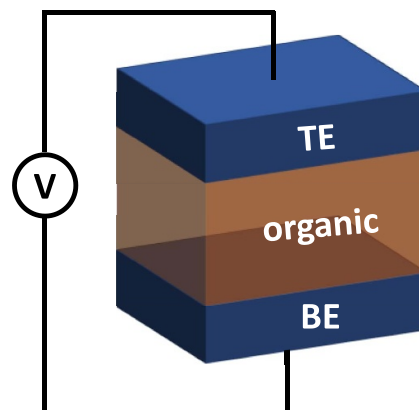


**Figure 3.** Schematic showing the simple structure of a single layer organic device. The switching matrix can be a range of thin-film organic materials, including small organic molecules or polymers in a thin-film or a monolayer of single molecules sandwiched between top electrode (TE) and bottom electrode (BE).

molecules, polymers, 2D organic materials (e.g. graphene) or a monolayer of molecules in the form of a self-assembled monolayer.

Prior to discussing single-layer organic memristors, it is worth mentioning that the first bistable organic resistive switching device, introduced in 2002 by Ma *et al* [46], incorporated a tri-layer structure (organic-metal-organic) that was deposited between two Al metal contacts. The same high dielectric constant organic material, 2-amino-4, 5-imidazoledicarbonitrile (AIDCN), was used for the two organic layers (50 nm thick for each) and these were separated by a thin Al metal film (20 nm) deposited between the two organic layers. Ma *et al*, ascribed the electrical bi-stability switching to a charging effect induced by the formation of nanoclusters within the intermediary Al layer [47]. Switching due to the formation of Al filaments was ruled out since the conductance of the device decreased with decreasing temperature, which is opposite to that expected for a metal. Since then, extensive efforts have investigated this resistive switching effect further as a means to better understand the switching mechanism and improve device performance. These studies have examined a range of materials including small molecule organic materials, polymers, and various organic–inorganic hybrid materials consisting of composites of metal or semiconductor materials dispersed within an organic matrix.

The demonstrated number of single layer based resistive memristors is significant. Some examples are summarised. A single layer bistable organic resistive memory was demonstrated [48] in a thin-film (400 nm) pentacene device with a structure of Al/C<sub>22</sub>H<sub>14</sub>/Al, figure 4(a). The device showed a bistable memory effect with an Off/On resistance ratio of about 10<sup>9</sup>. To clarify the bistable memory effect in the single layer devices, a tri-layer device structure of pentacene/aluminium/pentacene sandwiched between two Al electrodes was also fabricated. The same bistable memory behaviour was also observed in the tri-layer pentacene structure, also figure 4(a). It was found that the bistable switching effect in both structures exhibited a high conductance in the On state,

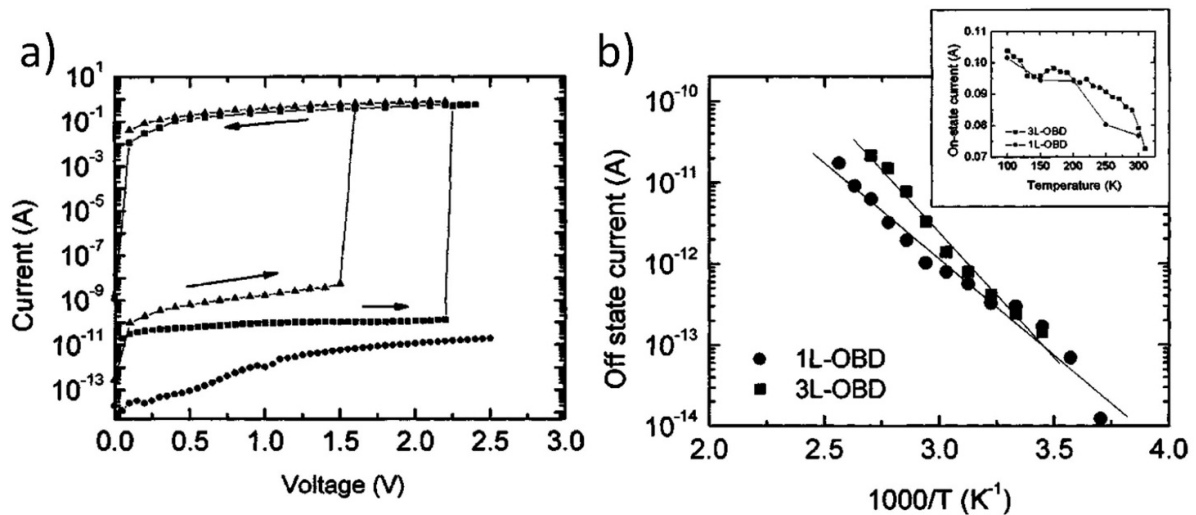


**Figure 4.** (a)  $I$ - $V$  sweeps for the single-layer (triangle dots) with a pentacene film of 400 nm and the tri-layer device (square dots) with the structure of pentacene (170 nm)/aluminium (20 nm)/pentacene (170 nm). Circle dots data (with no line) shows the  $I$ - $V$  curve for a single layer device (400 nm of pentacene) without the top Al electrode and mechanically contacted with a thin gold wire. In this case, no switching effects were observed. (b) Typical Arrhenius plots of the off-state current (measured at 0.1 V) for the same single-layer and tri-layer devices. Inset: current-temperature behaviours of the on-state current for both structures. Reprinted from [48], with the permission of AIP Publishing.

which led the authors to conclude that the resistive switching effect was due to the presence of Al NPs within the pentacene matrix. In the single layer device, it was expected that Al atoms diffuse into the organic layer during the Al top electrode evaporation process and aggregate to form NPs within the pentacene. Measurements on a single layer device using a gold wire as top contact instead of Al supported this hypothesis. However, for the tri-layer devices, the formation of the Al NPs was attributed to the middle Al layer which naturally forms NPs because of its very thin nature. Moreover, temperature dependent resistance measurements for the On and Off states for both device structures exhibited a metallic-like temperature dependence with a resistance that increased with temperature, figure 4(b). The hypothesis was that the applied electric field can modify the distribution of metal NPs, leading to formation of conducting nano-filament pathways through the organic layer and switching the device into the On state. However, switching off the electric field can relax the metal NPs, switching the device back to the Off state.

In another study based on single layer organic devices, a similar filamentary switching mechanism was observed that was instead found to be due to the formation of filaments that arose during the evaporation of the top Ag electrode [25]. Time-of-flight secondary ions mass spectrometry imaging was used to investigate metal diffusion and conductive filament formation in devices made from tris(8-hydroxyquinoline)aluminium ( $Alq_3$ ) sandwiched between ITO and Ag electrodes.  $Alq_3$  is a material of general interest in the field of organic electronics and has been broadly explored as an amorphous organic semiconductor for use in non-volatile memories. It was the first material to demonstrate organic non-volatile multi-bit storage ability [49] and it has exhibited both reliable unipolar and bipolar switching properties [50, 51]. It has also been widely used as an electron

transport layer in organic LEDs (OLEDs) [49]. In the study of filamentary switching in ITO/ $Alq_3$ /Ag devices the diffusion of Ag atoms in as-deposited (fresh) devices was discovered to be localised along statistically distributed paths rather than along a laterally averaged diffusion profile. Depth profile analysis showed that the  $Ag^{(-)}$  ions had diffused through the organic  $Alq_3$  layer (300 nm) to the bottom ITO electrode, most likely driven there as a consequence of field assisted diffusion processes during the deposition of the Ag top electrode, figure 5(a). It was also found that in as-deposited devices, conductive  $Ag^{(-)}$  filaments were present that had lengths up to 200 nm beneath the Ag/ $Alq_3$  interface. Electrical cycling between the LRS and HRS states indicated breaking and reforming of the filaments, as evidenced by changes in the  $Ag^{(-)}$  intensity close to the Ag/ $Alq_3$  interface and a rise in  $AgO_3^{(-)}$  and  $AgSO^{(-)}$  species, indicating inactivation of the filament by local oxidation. In the LRS state the conduction mechanism was ohmic but when the filament was ruptured to form the HRS state, conduction instead occurred by tunnelling, which pointed towards a conduction mechanism based on pathways consisting of multiple disconnected metal islands.

Many but not all organic and hybrid materials devices exhibit negative differential resistance (NDR) behaviour within their  $I$ - $V$  characteristics for a range of applied voltages higher than the threshold switching voltages [51]. NDR behaviour appears in devices that show a current decrease upon increasing applied voltage, typically after a SET process. The process occurs as follows. The devices are initially in the Off state and the current increases gradually with voltage. Once reaching the threshold voltage, the devices switch to the On state, followed by a local current maximum (when  $V = V_{max}$ ) and then a NDR region where the current decreases with increasing voltage. The devices have clearly distinguishable non-volatile HRS and LRS states for applied voltage values

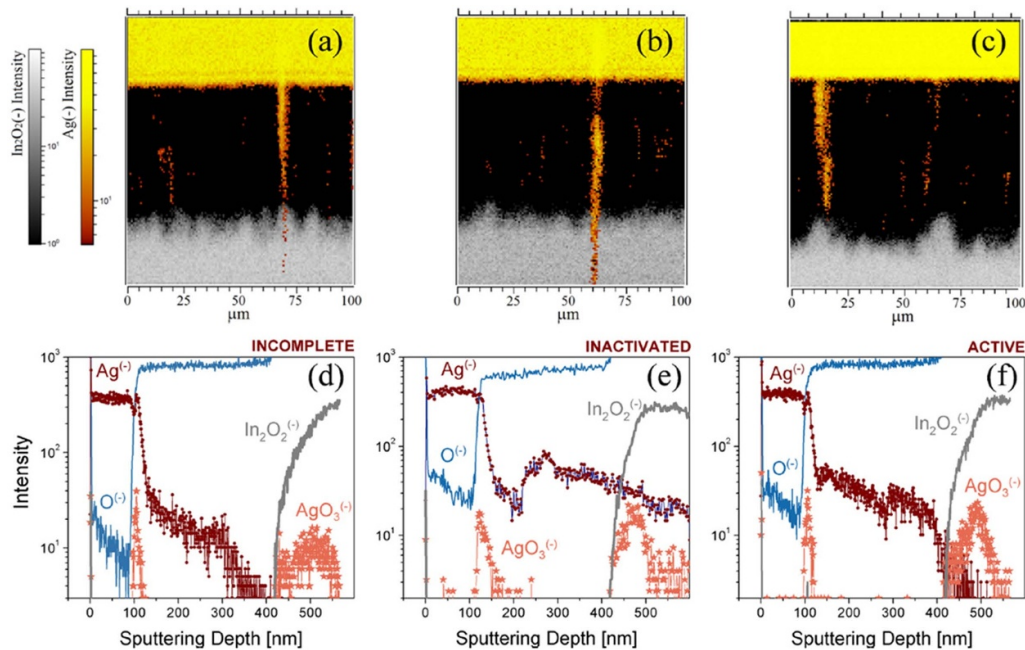


**Figure 5.** ToF-SIMS 3D imaging of ITO/Alq<sub>3</sub>/Ag memory device. The YZ cross section reconstruction shows the distribution of Ag<sup>(-)</sup> (top electrode) and In<sub>2</sub>O<sub>2</sub><sup>(-)</sup> (ITO) on CF region in (a) as-deposited, (b) cycled-HRS and (c) cycled-LRS devices. Panels (d)–(f) are the normalized depth profile reconstructions in the CF region. Oxygen and silver oxide/sulfide AgO<sub>3</sub><sup>(-)</sup> and AgSO<sup>(-)</sup> peaks (not separated) are displayed to visualize metal oxidation. The oxidation and drop of the Ag signal at the Ag/Alq<sub>3</sub> interface (panel (e)) are interpreted as an indication for filament breakdown. Reprinted from [25], with the permission of AIP Publishing.

lower than threshold voltages. Applying voltages above the NDR region switch the devices back to their Off states. NDR behaviour has been found in both bipolar and unipolar resistive switching devices.

The origin of hysteresis memory and NDR phenomena in single organic layer devices is still under debate, even though a considerable research effort has taken place to try and ascertain the origin of the phenomena. Fundamentally, two switching mechanisms have been applied in an attempt to explain the switching memory phenomena in single layer devices, namely nano-trap charging/discharging based processes and the formation and rupture of conductive filaments (filamentary switching). These two switching mechanisms are briefly discussed below.

### 3.1. Charging/discharging based memories

Some bistable memory and NDR effects have been attributed to the presence of metal NPs embedded within an insulating layer. The NPs can be mixed directly in solution within the material to be deposited or can be formed and diffused into the insulating layer during the deposition of the top electrode. The insulating materials can be small organic molecules (e.g. Alq<sub>3</sub>) or polymer materials (e.g. polystyrene). Non-volatile memory effects have also been reported in conjugated polymer systems, such as that shown in figure 6, where devices were made from the conjugated polymer polyaniline decorated with gold nanoparticles [52].

In the case of nanoparticles formed during the deposition of the top electrode, it has been reported that switching in both

small organic molecules and polymer materials is the same, even though they have very different nanoscale morphology [53]. The former material is amorphous in nature (when evaporated quickly), whilst the latter consists of a dense tangle of polymer chains. The research investigated Alq<sub>3</sub> and polystyrene as the small organic molecule and polymer material, respectively. ITO coated glass was used as the bottom electrode and thermal evaporation of the Al was used for the top electrode. TEM studies confirmed the existence of metal islands within the insulators and indicated that they formed and diffused there during the deposition of the top Al electrode. The devices showed a unipolar switching behaviour with NDR, resulting from a charging and discharging effect. Initially, the devices were in the Off state, and then switched into the On state when the bias was at the threshold voltage ( $V_{th}$ ). Charging was maintained by the high voltage applied up to  $V_{max}$ , however at voltages higher than this an NDR effect was observed. The system discharged completely when the applied voltage was switched off,  $V = 0$ , and returned the device back to the Off state. The characteristics of the  $I-V$  curves were similar to that observed in figure 6(b) for the polyaniline nanofiber/gold nanoparticle composite. Note that the  $I-V$  characteristics did not show a memory switching effect for devices fabricated by sandwiching the insulating matrix in between two preformed metal electrodes, which confirmed that the charging/discharging effect is induced by the diffused metal nano-traps formed during the thermal evaporation process.

The thickness and material characteristics of the insulator and the different formation and diffusion properties of the NPs

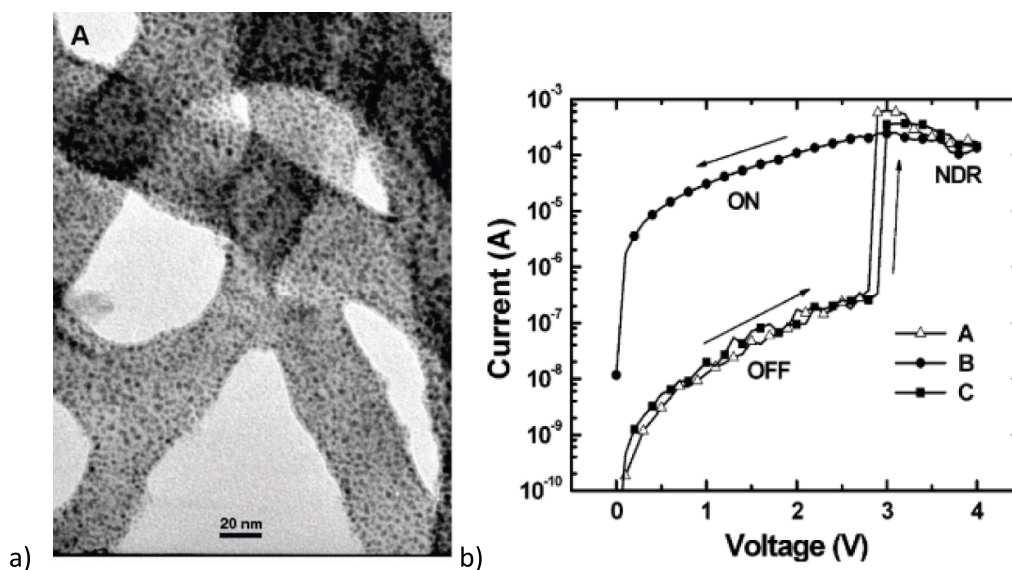


**Figure 6.** (a) TEM image of the polyaniline nanofiber/gold nanoparticle composite and (b)  $I$ - $V$  characteristics showing the non-volatile memory effect. NDR is also observed as the voltage is swept between +3 and +4 V. Reprinted with permission from [52]. Copyright (2005) American Chemical Society.

have a significant influence on the bistable memory effect in single layer devices. For example, it is found that the bistable memory effect induced by diffusion of Al NPs into pentacene in a Al/pentacene/Al device structure occurred with a pentacene thickness range between 150–600 nm [48]. Devices with pentacene thickness below 150 nm showed only a high conductivity (On) state, indicating a high amount of Al NP diffusion, whereas devices with pentacene thickness above 600 nm showed only a low conductance (Off) state and without switching into the On state even at higher applied voltages, indicating a low amount of Al NP diffusion across the pentacene layer. On the other hand, devices based on the Al/AIDCN/Al structure with an AIDCN (2-amino-4,5-imidazoledicarbonitrile) thickness of 50 nm did not show any bistable memory effects [46]. Switching was observed in AIDCN devices, but only when a thin Aluminium layer (acting as a charge trapping layer) was physically inserted between two 50 nm AIDCN layers. This result indicates that the formation and diffusion of Al NPs does not occur in AIDCN under these conditions (as it did for pentacene) and that one must be careful when applying similar processes to making devices with different organic materials.

The above studies highlight more generally the challenges in elucidating the mechanisms involved in these systems and the need for much more work to be done in this area (see recent review [54]). The problem is difficult, and understanding is exacerbated by the complex nature of organic materials themselves and their very different and wide-ranging properties. Organic materials can be electrically insulating, semi-conducting, highly conducting, and even have metallic-like conductivity [55]. They can have very different morphologies, and this can be important for devices properties at both the molecular and macroscopic level (e.g. highly crystalline, amorphous, polymeric (chains can be disordered or partially crystalline), granular, or have more complicated morphologies

as in composite materials where clustering, aggregation and phase separation can occur). The electronic levels (HOMO, LUMO) and polarizability of the molecules are important as well as the presence of chemical defects, electronic trap states and interfacial effects between the materials and contact electrodes. For device applications, the long-term stability of such systems and the influence of ambient conditions such as exposure to air and moisture [56, 57] are also important aspects to consider.

### 3.2. Conductive filament based memories

Bistable switching in organic memristors has also been explained by a filamentary switching mechanism, based on the formation and rupture of conductive filaments. Two types of conductive filaments have been reported, carbon-rich filaments formed by a local degradation of organic and polymeric materials, and metallic-like filaments formed by a redox reaction (also called electrochemical metallization (ECM)) of metal ions migrating from reactive electrodes. The latter has been reported in not only organic materials but also oxides and perovskites-based devices [58, 59], making it more common than carbon-rich filament formation. Fundamentally, ECM memory cells use a switching material, termed a solid electrolyte [60], sandwiched between an active metal electrode, e.g. Ag or Cu, and an inert electrode, e.g. Pt or W. The pristine ECM device is in a HRS state and a forming step is necessary to initiate the device. Application of a positive/negative voltage to the active/inert electrode ionizes the Ag atoms ( $\text{Ag}^+$  cations) at the Ag/organic or polymer interface. Under high electric field, the  $\text{Ag}^+$  migrates to the inert electrode, where the neutral Ag atoms are accumulated and begin forming a filament(s). Once the grown filament reaches the active electrode (Ag), the device switches into the On state (SET process). On the other hand, application of a negative voltage to

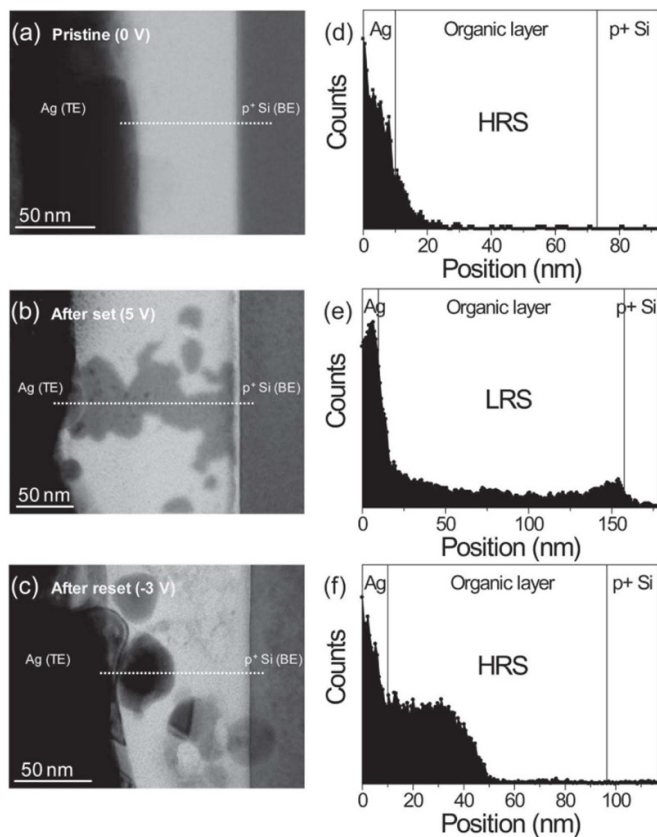


**Figure 7.** (a), (b), and (c) Cross-sectional TEM images of memory cells in the HRS (pristine), the LRS (after SET process at 5 V) and the HRS (after RESET process at  $-3$  V) states, respectively. (d), (e), and (f) EDX analysis for Ag element profiles along the dotted lines marked in (a)–(c). [61] John Wiley & Sons. [Copyright © 2011 WILEY-VCH Verlag GmbH & Co. KGaA, Weinheim].

the active electrode dissolves the formed filament, resetting the device into the Off state (RESET process). Note that, for unipolar switching memristors, the RESET process is instead induced by a Joule heating process, whereby a rupture of the conductive filament occurs at the narrowest region because of the high current [58].

Conductive Ag channels have been demonstrated in organic based memristors having the architecture of Ag/ WPF-BT-FEO polymer/heavily doped p-type Si [61]. The devices showed bipolar resistive switching with sharply transitioning SET and RESET processes at positive and negative voltage polarities, respectively. The conductive channels and their chemical composition for the pristine and cycled LRS and HRS states were investigated by TEM and EDX, as shown in figure 7. Initially, the pristine device showed a HRS at 0 V due to the absence of a conductive channel across the polymer layer. In this state, EDX measurements showed that Ag had penetrated into the polymer to a depth of about 10 nm during the evaporation of the top Ag electrode. Cycling the device between SET and RESET processes caused the formation and rupture of conductive channels (filaments) with a mechanism as follows: under the application of a positive voltage polarity on the top Ag electrode,  $\text{Ag}^+$  metal cations are formed and drift into the negatively biased heavily doped p-type Si

electrode, which causes the Ag conductive filaments to grow. The formation of Ag filaments is based on chemical oxidation and reduction reactions at the Ag/polymer and polymer/Si interfaces, respectively. The Ag filament continues to grow across the polymer layer (dark regions within the polymer layer, figure 7(b)) and connects the top and bottom electrodes, sometimes even extending into the bottom electrode, figure 7(e). This process sets the device into the LRS at a SET voltage of about 5 V. Under the application of negative voltage polarity, an electrochemical dissolution happens somewhere along the filament, breaking the channel between the two electrodes, figure 7(c), and switching the device into the HRS at the RESET voltage of  $-3$  V.

#### 4. Hybrid organic–inorganic nanocomposite devices

Hybrid organic–inorganic nanocomposites have recently emerged as potential candidates for flexible resistive switching memories owing to the benefits of combining the electronic properties of metals and semiconductors with the solution processing advantages of organic materials. These benefits include low cost, large area coverage on flexible and lightweight substrates, low temperature and vacuum free processing, and the use of simple fabrication techniques such as spin coating [36], screen printing or Langmuir–Blodgett methods [62]. Blending of metal NPs within an organic host matrix presents a simple way to fabricate hybrid resistive switching devices. A novel memristor, consisting of a polystyrene (PS) film having gold NPs and 8-hydroxyquinoline (8HQ) sandwiched between Al top and bottom electrodes, was demonstrated in 2004 by Ouyang *et al* [63]. The  $I$ – $V$  characteristics of the device are shown in figure 8. In its pristine form, the fabricated device exhibited a low conductance with a current of about  $10^{-11}$  A at a low applied positive voltage of  $\approx 1.5$  V. Once the applied voltage reached the threshold voltage of  $V_{\text{th}} = 2.8$  V, a sharp transition to higher conductance was observed with the current increasing to  $10^{-6}$  A, curve A. This high conductance state was maintained during the subsequent voltage sweep, curve B, showing a good stability of the device. However, the device abruptly switched back to its low conductance state upon application of a negative voltage of  $-1.8$  V, decreasing the current to  $10^{-10}$  A, curve C. Interestingly, the device showed very fast write/erase switching upon application of  $+5$  V/ $-2.3$  V pulses with a pulse width of 25 ns. This very fast, nano-second scale switching was attributed to an electric field induced switching mechanism in which the 8HQ and Au NPs act as electron donors and acceptors, respectively. At low applied positive electric field, the number of free carriers is small, resulting in a low conductance state. However, at high applied positive electric field, a charge transfer between the 8HQ and Au NPs takes place, charging the 8HQ positively and the Au NPs negatively. This field induced carrier generation process switches the device to the high conductance state. Upon the application of a negative electric field the process reverses, resulting in a switch back to the low conductance state.

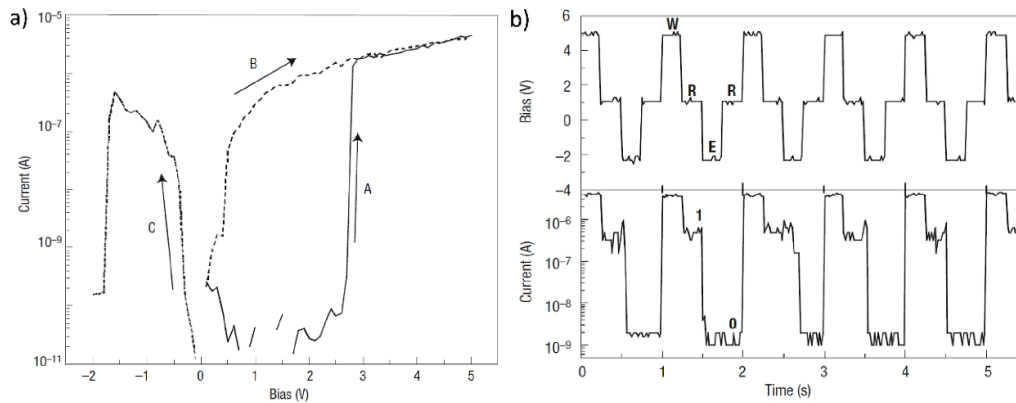


**Figure 8.** (a)  $I$ - $V$  characteristics and (b) write-read-erase cycles with ultra-fast nanosecond switching between low and high resistance states ( $<25$  ns) in an Al/Au NPs:8HQ:PS/Al device. Reproduced from [63], with permission from Springer Nature.

Flexible memristor devices based on a hybrid material of Au NPs embedded in poly (*N*-vinylcarbazole) (PVK) have been developed [11]. The hybrid material was sandwiched between an ITO coated poly(ethylene-terephthalate) (PET) substrate (bottom electrode) and Al (top electrode). The devices showed a bipolar switching effect with an Off/On resistance ratio of  $10^5$  and high endurance and retention performance of  $1.5 \times 10^5$  cycles and  $10^6$  s, respectively. The Off/On resistance ratio was found to be significantly dependent on the Au NP concentration, as illustrated in figure 9(b), where it is shown to increase with increasing Au NP concentration from 0.36% to 0.44%, and then decreased at 0.48%, because of the formation of Au agglomerations that diminish the trapping effect at the Au NP sites, thereby reducing the storage capability of the device. Capacitance-voltage ( $C$ - $V$ ) measurements on the devices, shown in figure 9(a), further confirm the trapping effect is induced by the Au NPs, since the hysteresis behaviour is only observed in the hybrid Au NPs:PVK system, while no hysteresis behaviour is observed in a control device consisting of only PVK film, inset figure 9(a).

More recently, memristor switching has been demonstrated in nanocomposites consisting of Au NPs suspended in graphene oxide (GO) films deposited between ITO and Al electrodes [64]. In this work, two device types were fabricated including a control device (GO without Au NPs) and the nanocomposite device (Au NPs:GO) with Au NP concentration of 0.05%. A forming process was needed to initiate the devices, ranging from 2 to 6 V depending on the Au NP concentration. A current limit of 1 mA was applied to prevent permanent breakdown. Both device types showed a bipolar switching behaviour with sharp SET transitions at positive voltage, as shown in figures 10(a) and (b). The embedded Au NPs in the GO act as trapping centres, which improved the Off/On resistance ratio up to 3 orders of magnitude in contrast to the control device, which showed an Off/On resistance ratio of about 1 order of magnitude. In addition, introducing the Au NPs improved the stability and uniformity of the relative fluctuations of the set voltage ( $V_{SET}$ )/reset voltage ( $V_{RESET}$ ) and resistance Off/On ratio (HRS/LRS), which reduced from 28.9%/47.3% (HRS/LRS: 32.2%/38.5%) to 11.2%/15.1% (HRS/LRS: 20.6%/5.9%), as

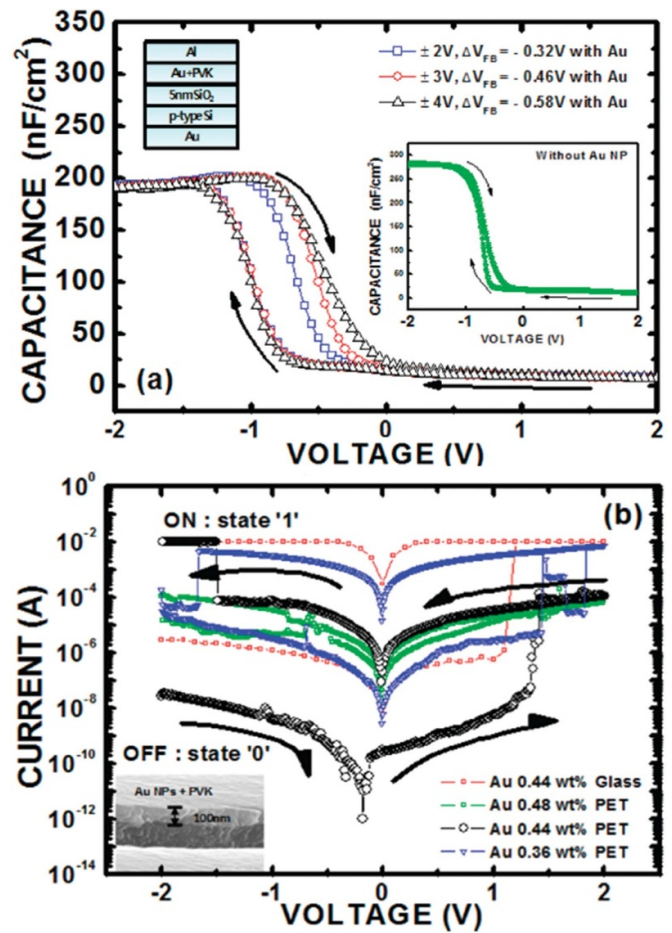


**Figure 9.** (a)  $C$ - $V$  measurements of Au/p-Si/SiO<sub>2</sub> (5 nm)/Au NPs:PVK/Al with a MIS structure at 1 MHz. The top left inset shows the fabricated device structure. The bottom right inset shows the  $C$ - $V$  curve for the control sample without Au nanoparticles. (b)  $I$ - $V$  characteristics of ITO/Au NPs:PVK/Al devices on PET and glass substrates. The inset shows the SEM cross-sectional view of the fabricated device. Reprinted with permission from [11]. Copyright (2010) American Chemical Society.

shown in figure 10(c) and (d). The improvement in the resistive switching properties was attributed to the change in the conductive path distribution formed during the LRS, which

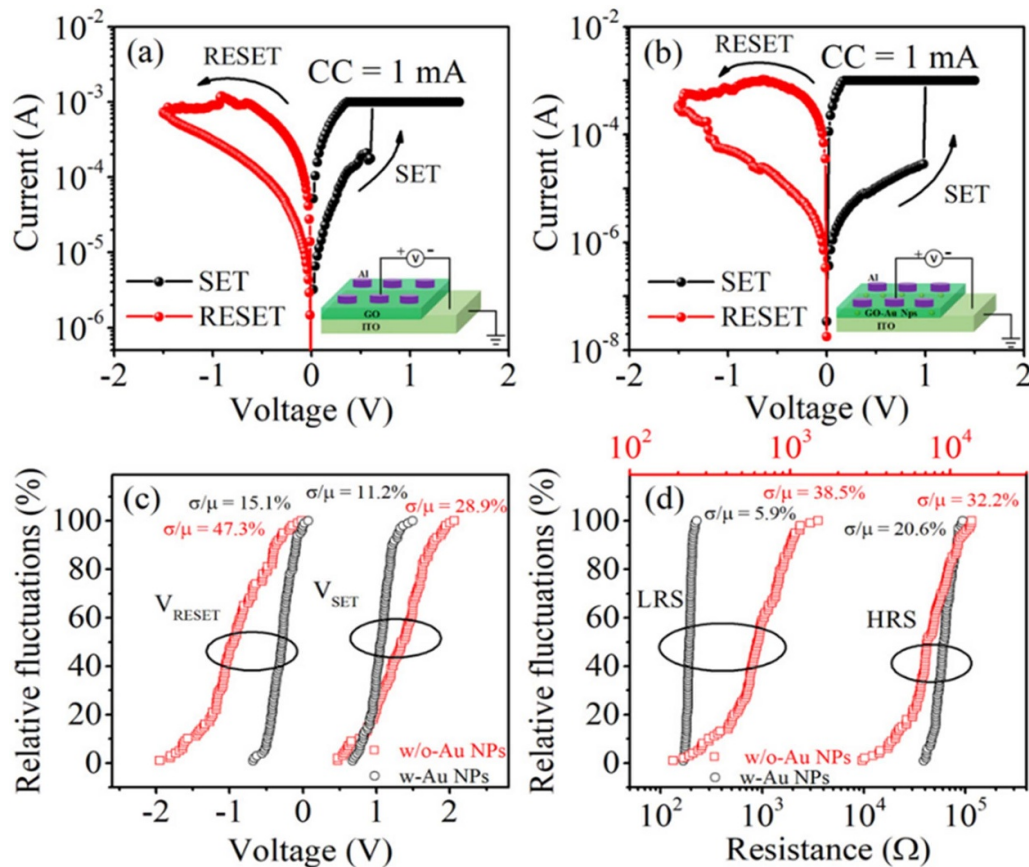


**Figure 10.** (a)  $I$ - $V$  characteristics of an ITO/GO/Al control device (without Au NPs). The inset shows the schematic device structure. (b)  $I$ - $V$  characteristics of an ITO/Au NPs:GO/Al hybrid device (with Au NPs). (c) and (d) Distributions of  $V_{SET}/V_{RESET}$  and HRS/LRS of 100 cycles for devices with and without Au NPs, respectively. Reprinted from [64], with the permission of AIP Publishing.

changed from being homogeneous in the control device to inhomogeneous (localised positions) for the hybrid Au NPs and GO device.

Similar improvement in the resistive switching properties has been observed in nanocomposites consisting of silver nanoparticles (Ag NPs) dispersed in PMMA [65]. The devices showed a HRS when the applied voltage was swept from  $+V_{Max}$  to  $-V_{Max}$ , with a smooth transition to the LRS after exceeding a critical amplitude of the applied voltage, figure 11. During the reverse sweep from  $-V_{Max}$  to  $+V_{Max}$ , the devices remained in the LRS and then switched back to its initial HRS at  $+V_{Max}$ . The device containing only a Ag NP thin-film deposited in between ITO and Al electrodes exhibited a low storage capacity as the Off/On resistance ratio was less than 1 order of magnitude (about 12), as shown in figure 11(a). However, the Off/On resistance ratio improved by 4 orders of magnitude in the nanocomposite device, see figure 11(b) where Ag NPs have been deposited within the PMMA material. The PMMA layer plays a key role in enhancing the Off/On ratio by controlling the resistance states. The PMMA polymer cannot be used alone however, since the memory effect is due to the presence of Ag NPs since no switching was observed in a device having only a PMMA layer. The bi-stability in the nanocomposite device and the pure Ag NP device is ascribed to the trapping and de-trapping effect. In

the case of the nanocomposite device, the charge carriers are trapped better because of the surrounding PMMA polymer, which limits leakage and discharge effect to the electrodes, resulting in a higher HRS in comparison with the device containing only Ag NPs.

Quantum dots (QDs) have emerged as an excellent material for potential memory and neuromorphic applications due to their unique tunable electronic and optical properties [66, 67]. Blending QDs in organic/polymer materials can be used to play a key role in modifying the RS characteristics of nanocomposite-based memristors. For example, a nanocomposite crossbar memristor device based on CdSe QDs (3.56 nm diameter) and poly(4-vinylpyridine) (PVP) sandwiched between Al electrodes, Al/CdSe-PVP/Al, has been synthesized [68]. The device exhibited robust  $I$ - $V$  bipolar resistive switching characteristics (150 sweeps), high Off/On resistance ratio ( $6.1 \times 10^4$ ), long retention (35 000 s), and low operating SET/RESET voltages ( $\pm 0.8$  V), figure 12. Additionally, the device showed ultrafast switching (41 ns) and ultralow power consumption of  $4.16 \mu W$  in the LRS and  $80$  pW in the HRS. These enhanced properties were attributed to the blending of CdSe QDs in the PVP polymer since a control device consisting of just the PVP film (Al/PVP/Al) showed poor switching and a low conductance even at high applied voltages ( $\pm 3$  V).

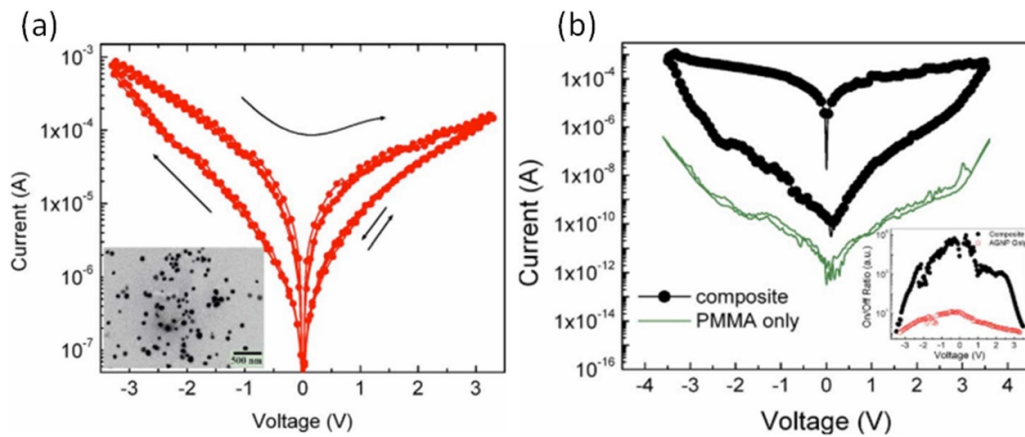


**Figure 11.** (a)  $I$ - $V$  characteristics of an ITO/Ag NPs/Al device. The inset shows TEM image of Ag NPs. (b)  $I$ - $V$  characteristics of a nanocomposite based device, ITO/PMMA:Ag NPs/Al, (black curve) and PMMA control device, ITO/PMMA/Al, (green curve). The inset shows the voltage dependence of the On/Off current ratio of both Ag NP based device and that of composite device. Reprinted from [65], with the permission of AIP Publishing.

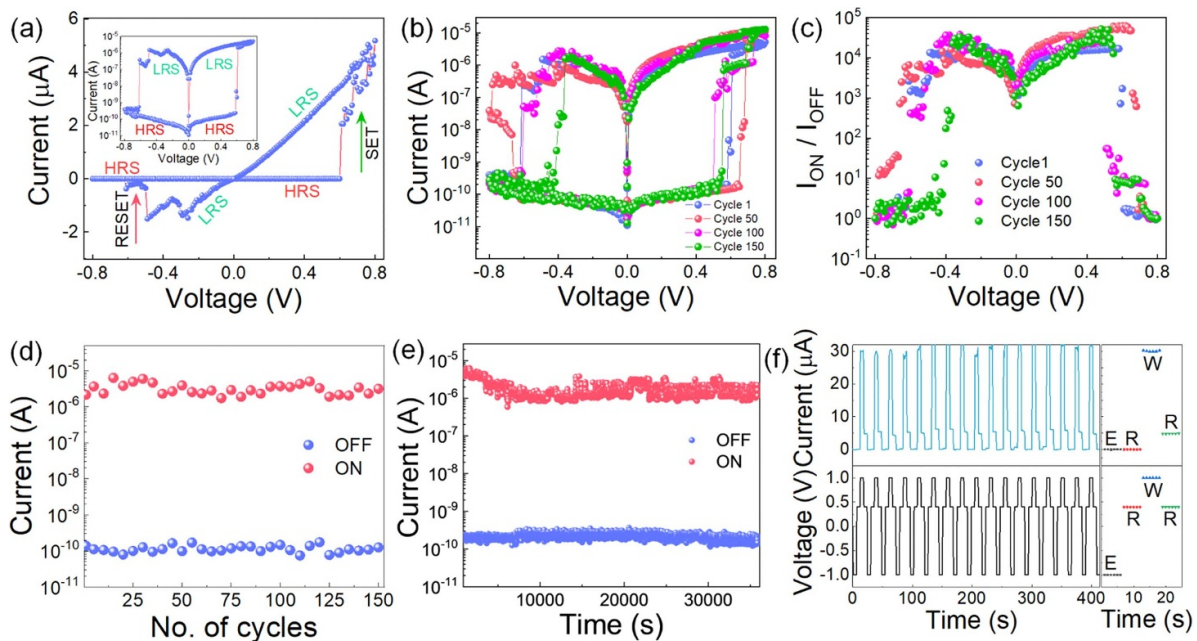


**Figure 12.** (a)  $I$ - $V$  characteristics of the Al/CdSe-PVP/Al device between  $-0.8$  V and  $+0.8$  V. (b)  $I$ - $V$  characteristics on a semi-log scale for the 1st, 50th, 100th, and 150th switching cycle. (c) Variation of  $I_{ON}/I_{OFF}$  with the applied voltage for the 1st, 50th, 100th, and 150th switching cycle. (d) Endurance test. (e) Retention test of the device at  $+0.4$  V. (f) RAM characteristic of the device. A sequence of pulses ‘erase ( $-1$  V)  $\rightarrow$  read ( $+0.4$  V)  $\rightarrow$  write ( $+1$  V)  $\rightarrow$  read ( $+0.4$  V)’ with a pulse width of 6 s each was applied. An enlarged view of one cycle is shown on the right-hand side where E, R, and W represent erase, read, and write, respectively. Reprinted with permission from [68]. Copyright (2022) American Chemical Society.

Recently, the optical properties of QDs have also been used to modify the resistive switching properties of hybrid QDs/polymer memristors. Chen *et al.* demonstrated an ultra-stable broadband photoelectric tunable crossbar memristor using hybrid PbS QDs dispersed in PMMA and sandwiched between ITO bottom and Ag top electrodes [69]. The device showed a photoelectric response in the spectral range between 405 nm and 1177 nm. Upon illumination within this spectral range, the device current increased from  $10^{-12}$  A to  $10^{-9}$  A and then decreased to  $10^{-12}$  A when the light was switched off (dark). Particularly interesting is that with illumination by

light of shorter wavelength, e.g. 405 nm, the operating SET voltage of the device decreased from 1.1 V to 0.25 V. The optoelectronic effect and the controlling of the SET voltages was ascribed to the creation of additional electrons and holes in the material, which better facilitated the formation of Ag conductive filaments across the device.

Recently, an investigation was carried out to understand contrasting views in the literature between studies that have used different nanostructured materials. Direct comparison of literature results has always been difficult as different research teams use different materials and processing techniques. With

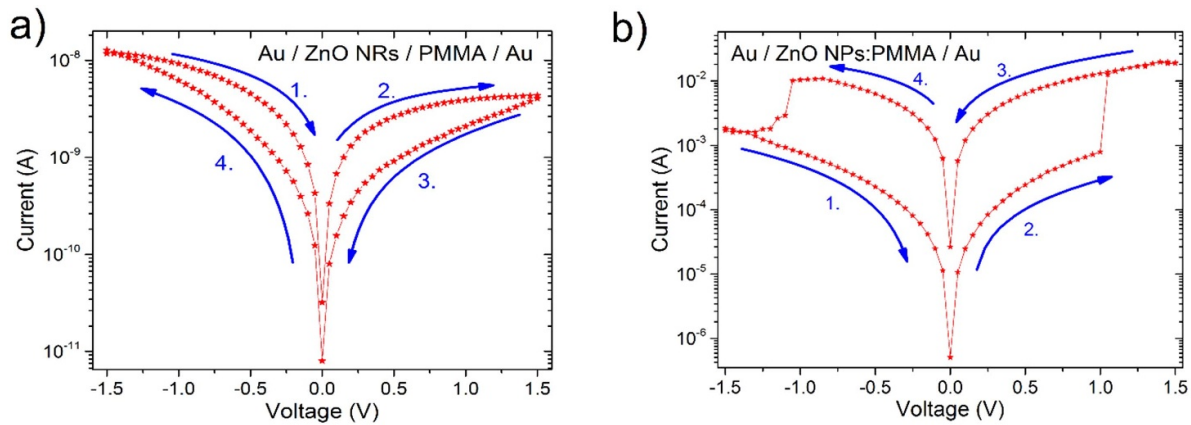


**Figure 13.**  $I$ - $V$  characteristics of (a) an Au/ZnO NRs/PMMA/Au device and (b) an Au/ZnO NPs:PMMA/Au device. © [2020] IEEE. Reprinted, with permission, from [34].

this in mind, nanostructured ZnO was examined in two forms, nanorods and nanoparticles [34], where both nanostructure geometries were embedded in a PMMA layer located between Au top and bottom electrodes in a crossbar structure giving the following device architectures, Au/ZnO NPs:PMMA/Au and Au/ZnO NRs/PMMA/Au. Both device types required no forming process to initiate switching and both exhibited bipolar switching behaviour at low applied sweeping voltage as shown in figure 13. The nanostructure geometry was found to have a significant effect on the switching properties and conduction mechanisms. For example, the hybrid ZnO NRs/PMMA based devices showed a smooth transition between the HRS and LRS with a low Off/On resistance ratio of about 30, figure 13(a). This contrasted with the observation of sharp transitions between the two states in hybrid ZnO NPs:PMMA based devices, which had instead a higher Off/On resistance ratio of about two orders of magnitude, figure 13(b). It was suggested that the smooth transition in the ZnO NRs devices was due to the existence of an insulating barrier region between the tips of ZnO NRs and the top Au electrode, which modulates the conduction mechanism from Poole-Frenkel to Schottky emission during switching from the LRS to the HRS and *vice-versa*. In contrast, the sharp transition in the ZnO NPs devices was attributed to a charge trapping/de-trapping effect and the formation of a space-charge field. In addition, the ZnO NR based devices showed an initially high conductance state, which indicates that the ZnO NR surface contained a large amount of surface defects (oxygen vacancies). In contrast, the ZnO NP based devices showed an initially low conductance state, which suggests the NPs are uncharged in their initial state.

Flexible memristors have been fabricated using GO in hybrid structures [70–75]. GO is considered an excellent candidate for future flexible and transparent electronic applications due to its high mechanical flexibility, high optical transparency, band gap tunability and low cost [71, 75]. A bistable electrical switching effect was demonstrated [70] in a 100 nm thick hybrid GO:PVK thin film sandwiched between ITO and Al electrodes. The device exhibited bipolar switching behaviour with an Off/On resistance ratio of about four

orders of magnitude, as shown in figure 14(a). The device also showed high-stability memory retention (up to three hours) and extremely high endurance (up to  $10^8$  cycles) for both On and Off states, figures 14(b) and (c). Similar results have also been reported by the same group for hybrid devices made from triphenylamine-based polyazomethine (TPAPAM) and GO thin film (50 nm thick) [76]. The switching processes between the On and Off states in both hybrid systems were explained by an intramolecular charge transfer (CT) interaction between the polymers and GO, which reduced the GO upon biasing the devices. In this scenario the polymer acts as a tunneling barrier for charge transport between the neighboring GO nanosheets and limits the electrical conductivity of the hybrid system. The devices in their pristine state were initially in the Off state. Once the applied voltage reached the switching voltage, transport of electrons from the peripheral vinylcarbazole groups into the GO occurred, resulting in a reduction of the GO. Electrons can propagate between the graphene nanosheets through a hopping process, which switched the system to the On state. On the other hand, reversing the applied voltage polarity removed electrons from the GO nanosheets, switching the system back to its initial Off state.

Modification of the resistance switching by dynamically changing the thickness of the active switching material has been reported [72] for a hybrid system consisting of GO flakes embedded in a polar beta-polyvinylidene fluoride ( $\beta$ -PVDF) polymer. The polar  $\beta$ -PVDF polymer is a ferroelectric/piezoelectric material that can contract/expand upon application of an external electric field. The devices were formed by depositing a 120 nm thick film of the hybrid ( $\beta$ -PVDF):GO material between ITO and Al electrodes. Bipolar resistive switching was observed, as presented in figure 15. The proposed model for the resistive switching mechanism was based on the change in dimensions of the hybrid system upon application of an external potential. It was expected that application of a positive electric field in the direction from the ITO to the Al contracted the hybrid material, which facilitated the formation of conducting pathway(s) between the two electrodes and resulted in a transition to the On state, figure 15(b). Conversely,

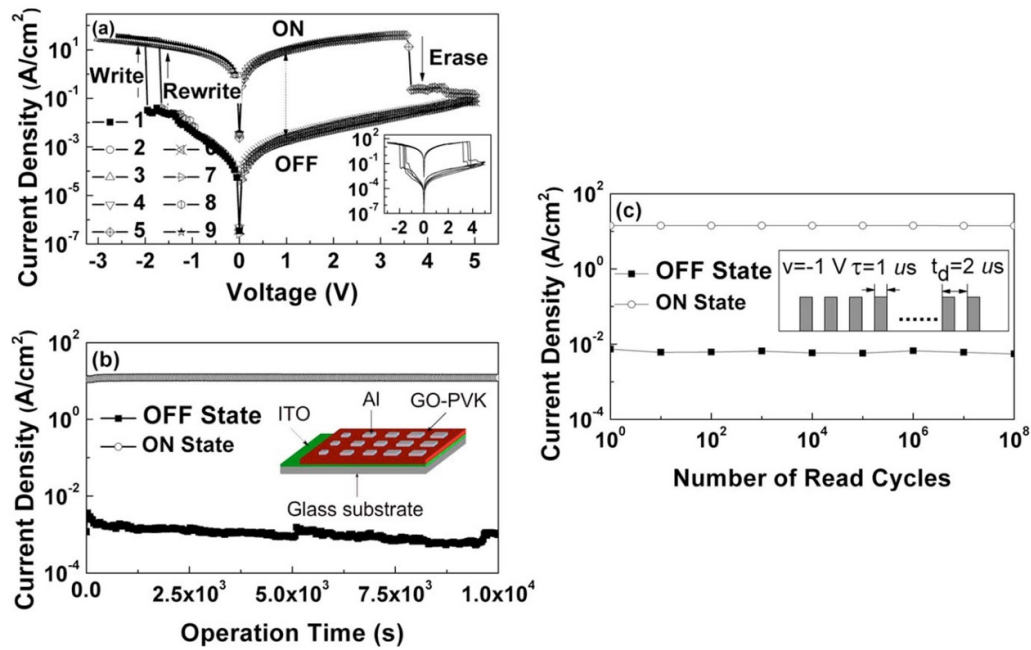


**Figure 14.** (a) J-V characteristics of the Al/GO-PVK/ITO device. The inset shows three write-read-erase-read-rewrite cycles. (b) Retention measurements for the On and Off states of the Al/GO-PVK/ITO device under a constant stress of  $-1 \text{ V}$ . (c) Endurance measurements under a continuous read pulse with a peak voltage of  $-1 \text{ V}$ , a pulse width of  $1 \text{ } \mu\text{s}$ , and a pulse period of  $2 \text{ } \mu\text{s}$ . The inset shows the voltage pulses employed for the device stability test. Reprinted from [70], with the permission of AIP Publishing.

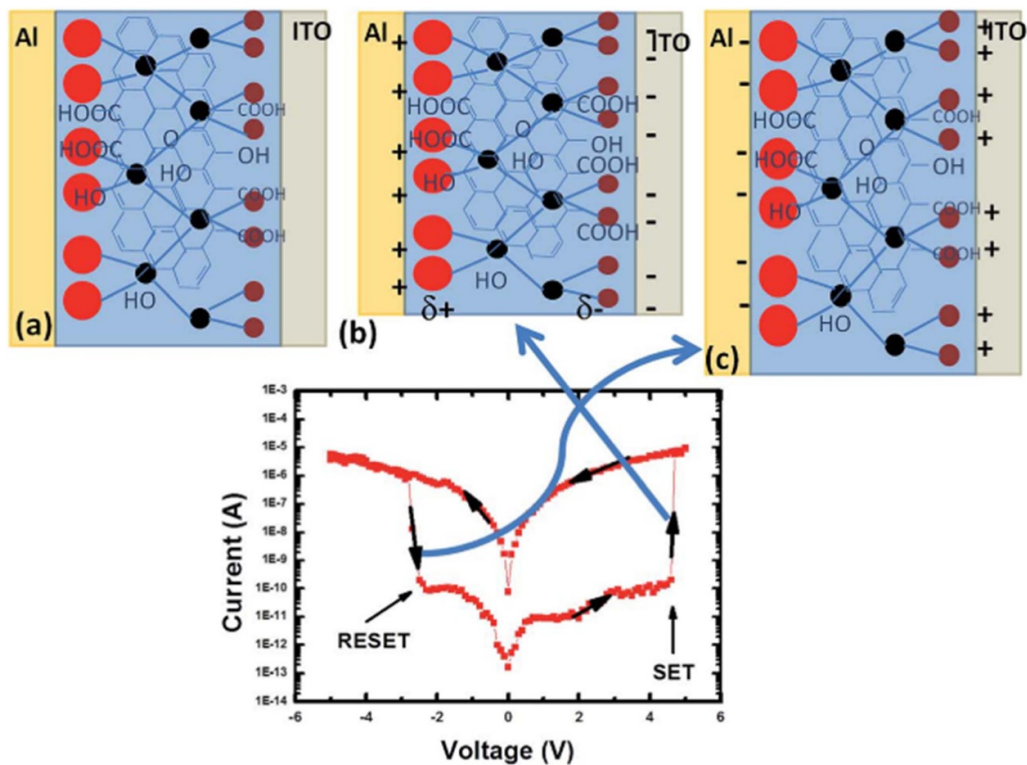


**Figure 15.** Representation of the model which demonstrates the shape and size of the  $\beta$ -PVDF:GO composite under application of an external E-field, (a) before the SET E-field, (b) near and above the breakdown SET E-field (polar PVDF contracts under positive E-field), and (c) near and just below the RESET negative E-field (polar PVDF expands under negative E-field). The I-V cycle indicates the SET and RESET processes with a possible piezoelectric based model. Reproduced from [72] with permission from the Royal Society of Chemistry.

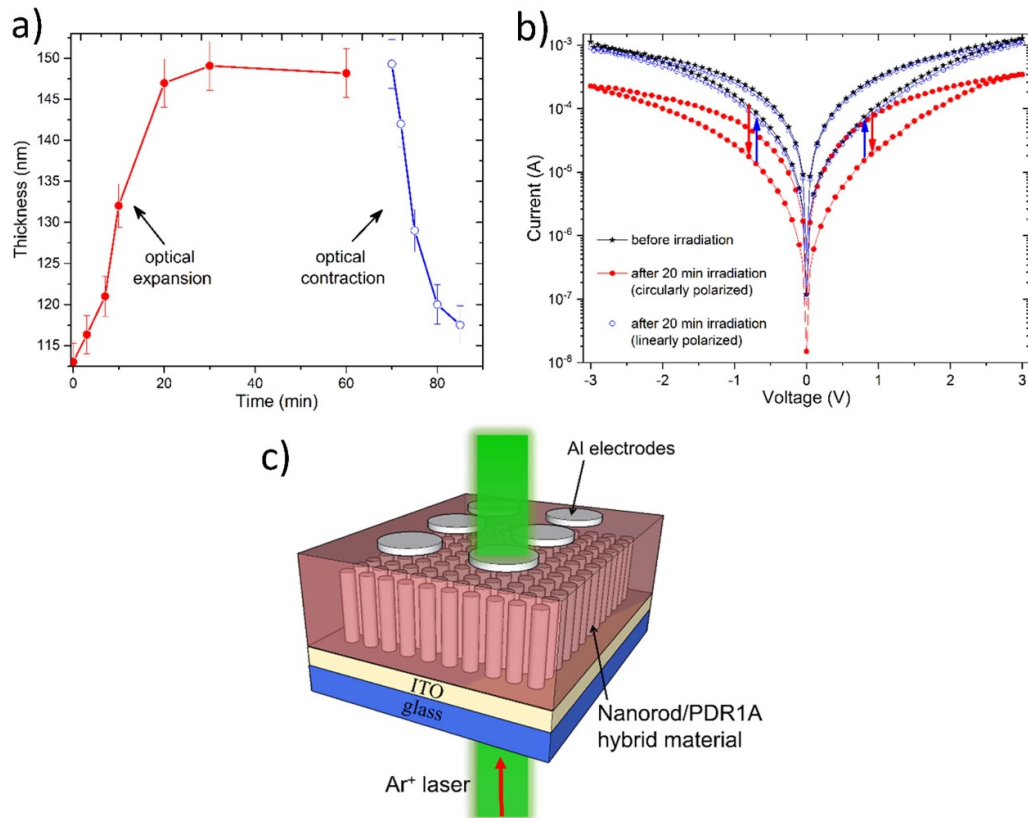


**Figure 16.** (a) Expansion (red curve) and contraction (blue curve) of the PDR1A film upon irradiation with circularly and linearly polarized light, respectively. (b) Optical modulation of the  $I$ - $V$  properties before irradiation (black), directly after irradiation with circularly polarized light (red) and after linearly polarized light (blue). (c) Schematic of the optical resistive switching memory. Reproduced from [77] with permission from the Royal Society of Chemistry.

application of a negative electric field expanded the layer, rupturing the charge carrier's pathway(s), and hence resetting the device to the Off state, figure 15(c).

The control of resistive switching by optical means has been demonstrated in a hybrid (organic–inorganic) composite system containing ZnO NRs embedded in poly(disperse red 1 acrylate) (PDR1A) matrix [77]. PDR1A is an optically active azobenzene polymer, which can expand and contract upon irradiation with wavelength- and polarisation-specific light. The ZnO NRs (about 200 nm length) were grown vertically onto ITO coated glass substrates by a hydrothermal assisted microwave technique. After this, PDR1A (110 nm thick) was deposited onto the ZnO NR film followed by deposition of top Al electrodes to give the device structure of ITO/ZnO NR/PDR1A/Al. The entire solution-based process offers a simple and low-cost route for the fabrication of optically tuneable memristor devices.

The reversible change in thickness of PDR1A upon irradiation controlled the resistance of the hybrid system. The thickness of PDR1A can be expanded up to about 30% upon irradiation with circularly polarised light ( $\text{Ar}^+$  laser, 514 nm) for 20–30 min and contracted back to its initial thickness upon irradiation with linearly polarised light ( $\text{Ar}^+$  laser, 514 nm) for 15 min, as can be seen in figure 16(a). In their pristine state, devices exhibited typical bipolar switching with an Off/On resistance ratio of about 10 during sweeping between  $-3$  V and

3 V, black curve in figure 16(b). Illumination of the device with circularly polarised light for 20 min expanded the thickness of the PDR1A film, resulting in an increase in the resistance of the device and a shift in the entire  $I$ - $V$  curve to lower value, red curve in figure 16(b). In contrast, illumination of the device with linearly polarised light for 15 min contracted the PDR1A film to its initial thickness, decreasing the resistance of the device and shifting the  $I$ - $V$  curve to its original value, blue curve in figure 16(b). The smooth transition between On and Off states was associated with the migration of oxygen vacancies at the tips of the ZnO nanorods [77]. Similar approaches have since been used to control the resistive switching properties of memristor devices by optical means using gold Au NPs [16], ZnO NPs [78] and  $\text{TiO}_2$  NRs [79] embedded in PDR1A.

#### 4.1. Effect of loading content

The loading content in hybrid organic–inorganic nanocomposite memristors has a significant effect on the resistive switching properties. For instance, changing the concentration of nanoparticles within the host matrix controls the Off and On resistance values and their Off/On resistance ratio. The effect of loading concentration on the resistive switching properties has been studied in nanocomposites consisting of ZnO NP embedded in PMMA [34]. In this study, different concentrations of ZnO NPs:PMMA were used ranging from mass

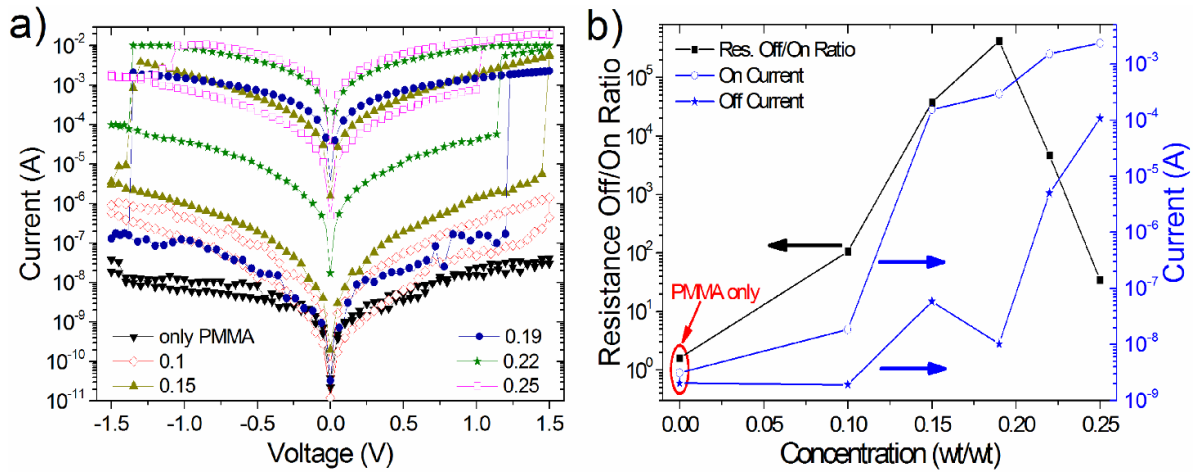


**Figure 17.** (a) *I*-*V* characteristics of a hybrid organic-inorganic nanocomposite memristor (ZnO NP: PMMA) with different NP loading concentrations. (b) Plot of the Off/On resistance ratio (left axis) and On and Off currents as a function of ZnO NP concentration (right axis). © [2020] IEEE. Reprinted, with permission, from [34].

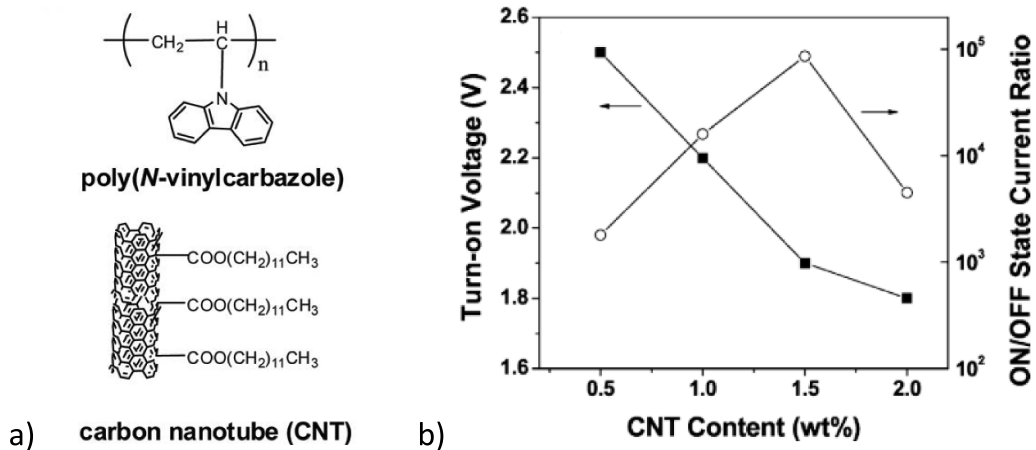


**Figure 18.** (a) Structure of the poly(N-vinylcarbazole) carbon nanotube composite material and (b) SET voltage (left axis) and On/Off state current ratio of the ITO/PVK:CNT/Al devices (right axis). Reprinted with permission from [80]. Copyright (2009) American Chemical Society.

fraction 0–0.25, as shown in figure 17. It was found that the resistive switching effect was either not observed or is greatly diminished at both low and high NP concentrations. At very low NP concentration, charge storage cannot occur in the devices, whereas at high concentration either the charge dissipates away to the electrodes or there is a localised conducting pathway between the two electrodes, causing a short-circuit. Between the low and high concentrations there is an optimum concentration where the resistive switching effect is maximized. In the ZnO:PMMA system investigated, this occurred at the ZnO:PMMA mass fraction of 0.19. This can be seen in figure 17(b), which shows the current of the On and Off states as a function of the NP concentration on the right axis and the calculated Off/On resistance ratio on the left axis. The graph clearly shows the On and Off currents are increased with increasing NP concentration. In addition, the Off/On resistance ratio reached a maximum of about 4 orders of magnitude at the mass fraction of 0.19, and then decreased at higher

NP concentration. The latter occurring because of increased particle-particle tunnelling at reduced NP separation.

Varying the NP loading in the host matrix also controls the SET voltage. This was shown in the above study as well as others [16, 80]. In one study, memristor devices consisting of carbon nanotubes (CNTs) embedded in a poly(N-vinylcarbazole) (PVK) host polymer with a device structure of ITO/CNT:PVK/Al were investigated [80]. In these devices, the SET voltage (turn-on voltage) decreased from 2.5 V to 1.8 V by increasing the CNT content from 0.5 to 2%, as shown in figure 18. Increasing the CNT loading from 0.5%–2% decreased the average distance between the nanotubes from 150 nm to 15 nm, which reduced the activation energy for effective charge hopping and the threshold switching voltage. The plot also shows that the On/Off current ratio is maximised at a CNT loading of 1.5% (wt).

The loading content not only controls the RS properties, but also tunes the electrical conductivity of nanocomposite

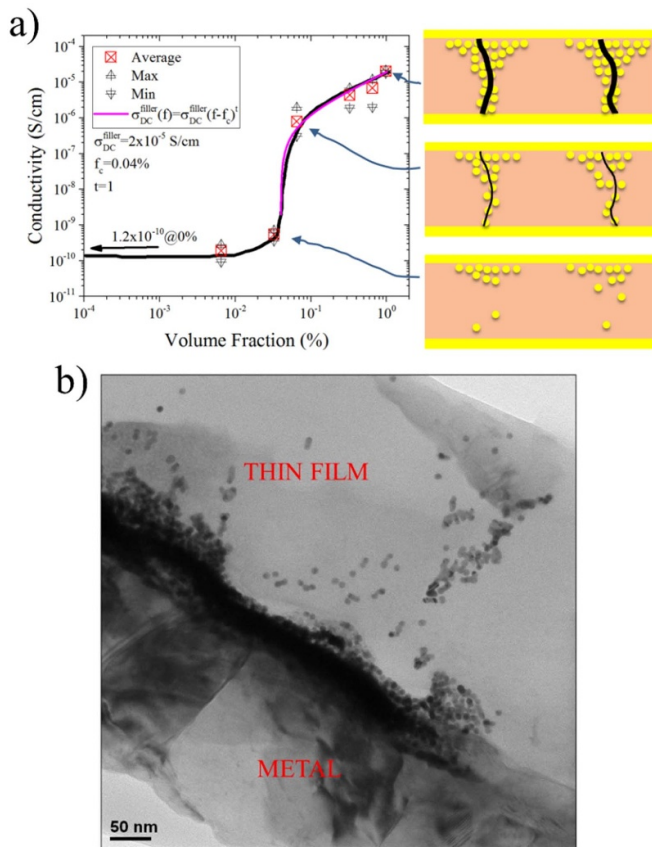


**Figure 19.** (a) Conductivity versus Au NP volume fraction in PDR1A. At each volume fraction, the data points shown in the graph represent the average, maximum, and minimum conductivity of the nanocomposite film. The black curve represents a guide to the eye for the trend. The pink curve represents a plot of the supercritical function showing a good match to the experimental percolation regime, assuming a percolation threshold of 0.04% and a supercritical exponent  $t = 1$ . The images illustrate the segregation of NPs below, at and above percolation threshold. (b) TEM image of an annealed thin film of Au NPs dispersed within PDR1A at a volume fraction 0.065% and showing the inhomogeneous distribution of NPs and the development of a filamentary pathway extending across most of the bulk film. [16] John Wiley & Sons. [Copyright © 2019 WILEY-VCH Verlag GmbH & Co. KGaA, Weinheim].

systems. In a unique system consisting of Au NPs dispersed in an optically active polymer, poly(disperse red 1 acrylate) (PDR1A), the electrical conductivity of the nanocomposite as a function of the Au NP volume fraction has been studied [16]. It was found that the electrical conductivity sharply increased, up to three orders of magnitudes, when the Au NP volume fraction increased from 0.033% to 0.065%, as shown in figure 19(a). This increase in the conductivity is expected from the physical phenomenon of inhomogeneous percolation, in which above a certain critical threshold, conducting Au NPs form conductive nanochannels in the inert PDR1A matrix. Below threshold, the Au NP volume fraction is too low to bridge the thin film, whereas above threshold, one or more bridging paths can form across the thin film as shown in the TEM image for the nanocomposite thin film with Au NP volume fraction of 0.065%, figure 19(b).

## 5. Memristor printing technologies and benefits

There is increasing interest in constructing new printed electronic devices on flexible substrates for applications where it is necessary that the material can fold, bend and sometimes even stretch [81]. This new form of electronics offers new product paradigms (e.g. wearable electronics) that are not possible with the use of conventional semiconductor devices which require rigid substrates. Printed electronics offers the advantages of simple fabrication technologies with low capital and materials costs, as well as substrates such as plastics and textiles that are lightweight [82]. Since computer memory is a fundamental element of almost all modern-day electronics [83], the fabrication of high-performance printed memory components such as memristors on flexible substrates is also important. However, most existing memristor devices use materials that require deposition techniques such as thermal evaporation, sputtering, atomic layer deposition and pulsed laser deposition [84–87]. These techniques require high vacuum conditions and/or high temperatures, which make them unsuitable for many of the lightweight and flexible substrate materials such as polymers and fabrics. The methods are also costly and not suitable for large volume, high throughput, or large-area fabrication. Printing technologies based on solution processing are however well-recognized deposition techniques that can address the above-mentioned issues.

Printing technologies can be categorised into two main types: in-contact and non-contact techniques. For in-contact techniques, the printing plate is in direct contact with the substrate. These techniques include screen printing, flexography, gravure printing and soft lithography. For non-contact techniques, only the printed materials are in contact with the substrate and these techniques include aerosol and inkjet printing. Each of these techniques has its own advantages and disadvantages. In the case of contact printing technologies, screen printing offers speed and versatility for planar and roll-to-roll printing processes. However, it suffers from low resolution under  $30 \mu\text{m}$ , large waste production and is not suitable for low viscosity inks [88]. Flexography and gravure techniques provide low cost and high speed and are better than the latter for high quality patterns and low viscosity inks [88, 89]. However, the halo effect (patterns with excess of ink) and cylinder life are considerable limitations for the flexography printing and gravure printing, respectively [89–91]. For non-contact printing, aerosol and inkjet techniques can be used for many types of materials and substrates. Aerosol printing is more applicable for complex designs and low temperature processing, whereas inkjet printing is more suitable for low viscosity solutions and situations where it is important to minimize waste. Aerosol and inkjet techniques, however, have the limitation of low-quality patterning and slow speed, respectively [92–95].

To date most organic and hybrid organic–inorganic composite memristors reported in the literature have been fabricated on rigid substrates using spin coating and drop casting techniques. This is often done for reasons of simplicity and efficiency in research, since it provides a quick way to

make a small number of devices for testing and characterisation purposes. Although these are not printing techniques, the materials used can often still be used in conventional contact and non-contact printing methods. If this is not the case then spin coating and drop casting techniques still have solution processing advantages such as high-speed vacuum free deposition in ambient conditions at low cost [37, 52, 96, 97]. In the following we discuss a few literature reports in which memristor devices have specifically been printed onto flexible substrates.

Printed memristors based on organic and hybrid organic–inorganic composites have demonstrated reliable and reproducible memory properties in terms of write/erase operation speeds, retention and endurance capabilities, large Off/On resistance ratios, small switching voltages and good scalability and mechanical flexibility [33, 71, 75]. Flexible polymer-based crossbar memristor devices (Ag/Nafion/Au) have been fabricated on polyethylene terephthalate (PET) substrate using an electrohydrodynamic (EHD) printing technique [98]. These devices were forming-free, exhibited typical threshold voltage switching behaviour and have been employed in a leaky integrate and fire neuron circuit. The printed array showed a good device-to-device uniformity with a yield of 93%, demonstrating that EHD is a viable approach for fabricating uniform flexible memristor devices. The devices also showed stable threshold switching under mechanical flexing (up to 100 cycles) and high temperature conditions (up to 125 °C). The resistive switching mechanism in these devices was attributed to the formation and spontaneous rupture of Ag filaments across the device.

All-printed memristor devices based on a perovskite  $\text{ZnSnO}_3$  and polyvinyl alcohol (PVOH) nanocomposite material have been reported by Siddiqui *et al* [99]. The nanocomposite material and Ag top and bottom electrodes (Ag/PVOH:ZnSnO<sub>3</sub>/Ag) were deposited on flexible PET substrates *via* the EHD method with reverse offset printing. The device showed a non-volatile bipolar resistive switching memory effect. With a positive applied voltage, the device initially existed in the HRS until a SET process took place at about 1.5 V. Reversing the applied voltage switched (RESET process) the device back into its HRS at about –1.5 V. The device also showed a good stability for retention and endurance tests and significant mechanical flexibility upon repeated bending (up to 1500 cycles) to a radius of 15 mm.

Printed memristors based on metal-oxides have also been demonstrated [100, 101]. A fully printed memristor on a paper substrate using a sequence of screen-printing and inkjet printing technologies has been reported [100]. The devices were made from a resistive switching  $\text{TiO}_2$  ink deposited *via* inkjet printing and used a carbon bottom and Ag top electrode (Ag/ $\text{TiO}_2$ /C) that were deposited *via* screen-printing. The devices required no forming process and showed reproducible bipolar switching, good retention and endurance capabilities, a tunable resistance Off/On ratio (achieved by controlling the  $\text{TiO}_2$  thickness), and the ability to operate under bending conditions. Moreover, the memristors were printed onto items and living objects for multifunctional, wearable, on-skin and bio-compatible applications as shown in figure 20. The paper

memory device labelled onto undeformed hand skin exhibited repeatable switching for 1000 cycles and operated normally under compressed and stretched skin condition wears. For long-term use there was also no skin irritation.

It is worth mentioning that printed memristors fabricated on rigid substrates have also been reported in the literature. For instance, inkjet-printed 2D materials-based memristors [102], fully printed memristors made from Cu-SiO<sub>2</sub> core-shell nanowire composites [21], and bilayer printed memristors based on two organic polymers (MEH:PPV and PMMA) [103]. All of these device types were fabricated on glass substrates but could easily have been deposited on flexible substrates since the materials and fabrication methods used are compatible with flexible substrates.

## 6. Flexible neuromorphic memristors for computing applications

In this last section the use of printed and flexible memristors in the exciting new field of neuromorphic computing is discussed. Here the benefits of lightweight, ultra-thin and flexible devices would permit new high-performance and energy efficient neuromorphic computing devices for use in applications such as portable devices and wearable electronics.

The fabrication and integration of artificial synapses as both memory and computing elements in neuromorphic and mem-computing applications is emerging as a viable approach to overcome the bottleneck limitations of traditional von Neumann computing and the recent scaling problems of semiconductor structures associated with the end-of-Moore's law computing [104]. Memristors have emerged as next generation memory devices for neuromorphic computing systems since they emulate the analogue switching and learning characteristics of biological neural synapses [105]. Memristors with their simple, two-terminal structure and crossbar architecture can be designed to function as artificial synapses and achieve similar learning and memory properties of biological synapses. Hebbian theory postulates that biological synapses can learn upon adapting to repeated signals/pulses [106]. Synaptic plasticity is a measure of this response over time and involves either a weakening (depression) or strengthening (potentiation) of the synaptic connection. In the case of a memristor, the synaptic plasticity is a measurement of its electrical conductivity [77]. Memristors in their initial state show relatively low conductivity. Upon application of a series of successive external electrical stimuli of a given polarity (or optical pulses in some cases), the conductivity of the memristor increases. This can be considered as a potentiation of the synaptic plasticity. Changing the polarity of the external stimuli and applying a series of successive pulses decreases the conductivity of the memristors. This causes depression of the synaptic plasticity. Figure 21 shows the potentiation and depression behaviour of a flexible artificial synapse consisting of a resistive switching material based on the 3D organic biopolymer, lignin. The biocompatible and biodegradable lignin polymer that is derived from wood, was sandwiched between ITO and Au electrodes and deposited onto a flexible PET substrate.

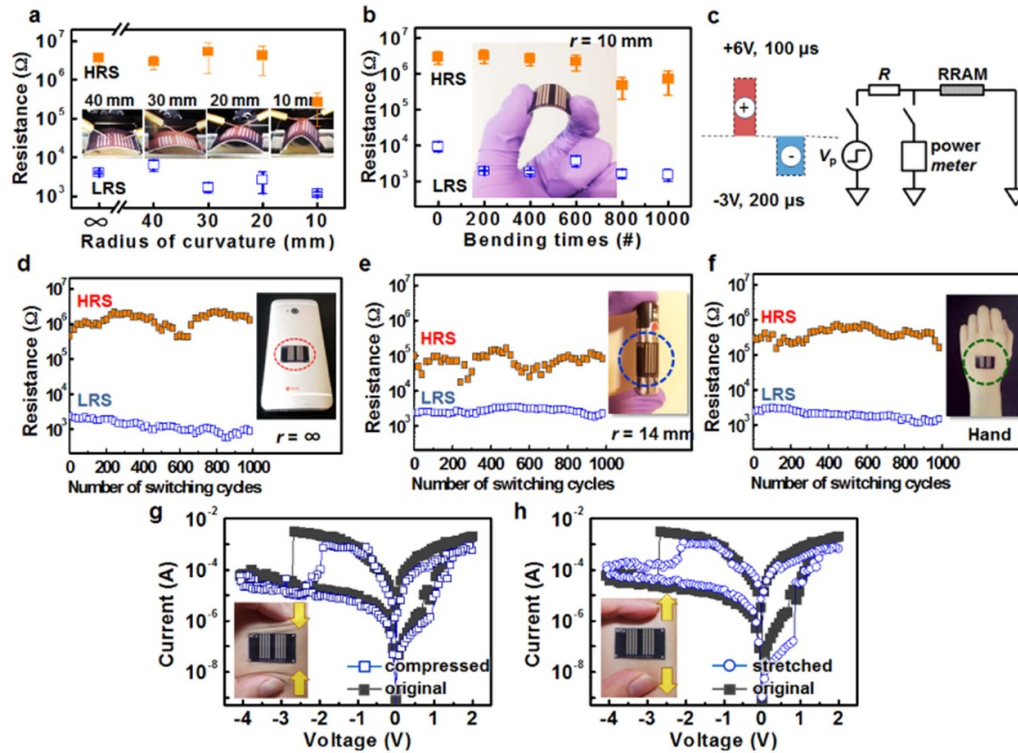


**Figure 20.** Bending test and on-chip and on-skin applications. (a) Off/On resistances as a function of bending radius of curvature. The inset shows a series of images of the device under different bent conditions. (b) Off/On resistances as a function of bending time with a bending radius of  $\sim 10$  mm. (c) Illustration of the equivalent circuit for the pulse measurement system. The inset illustrates the condition of the input pulse, which is composed of a 100  $\mu$ s duration, 6 V pulse for the write operation and a 200  $\mu$ s duration, 3 V pulse for the erase operation. The reading voltage used was 0.5 V. The switching characteristics of memory labels tagged on (d) a smart cell phone (flat surface:  $r = \infty$ ), (e) an AA battery ( $r = 14$  mm), and (f) undeformed skin of the human body. The switching characteristics of the paper memory on (g) compressed and (h) stretched skin of the human body. Reprinted with permission from [100]. Copyright (2014) American Chemical Society.

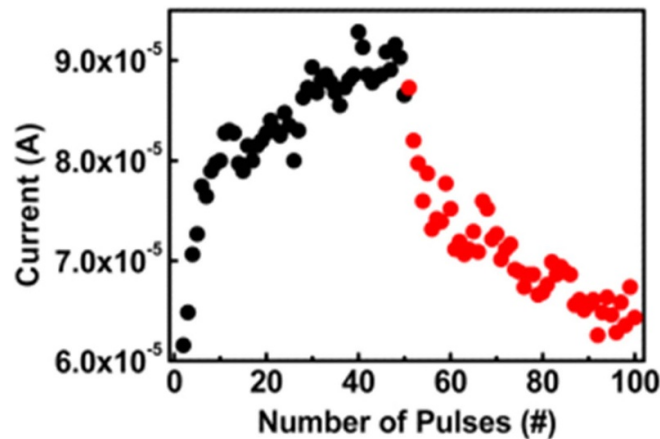


**Figure 21.** Classical habituation phenomenon controlled by electrical pulses in an artificial synaptic device and showing the incremental increase (potentiation) and decrease (depression) of the current. Reprinted with permission from [107]. Copyright (2017) American Chemical Society.

The device was potentiated by applying 50 consecutive negative pulses ( $-0.7$  V) with pulse width of 100 ms, and depressed by the application of 50 consecutive positive pulses ( $+0.7$  V, 100 ms) [107]. The device also exhibited short- and long-term memory effects and operated with good stability when the substrate was bent.

Spike-timing-dependent plasticity (STDP) is also a key tenet of Hebbian learning and has been linked with sensory perception, spatial reasoning, language, and conscious thought in the neocortex [108]. In STDP, learning and data storage depends on the modification of the synaptic weight in response to timing ( $\Delta t$ ) between action potentials from

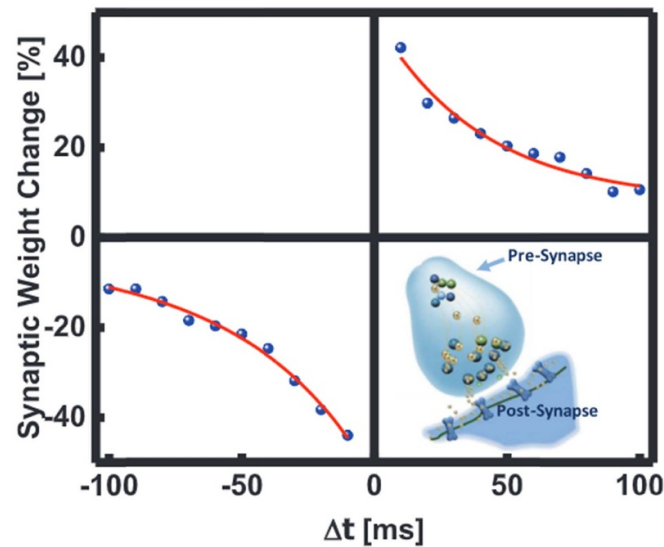


**Figure 22.** Spike-timing-dependent plasticity (STDP) of the collagen-based artificial synapse. The inset shows a schematic of the biological synapse. [110] John Wiley & Sons. [Copyright © 2018 WILEY-VCH Verlag GmbH & Co. KGaA, Weinheim].

neighbouring neurons, called pre-synaptic and post-synaptic spikes. The arrival of overlapping pulses can strengthen the synaptic weight (potentiation) if the pre-synaptic pulse arrives before the post-synaptic pulse, or weaken the synaptic weight (depression) if the post-synaptic pulse arrives before the pre-synaptic pulse. In the case of memristors, the desired synaptic weight is achieved by applying pre-synaptic and post-synaptic spikes separated in time ( $\Delta t$ ) [77, 109]. Raeis-Hosseini *et al* demonstrated flexible and transparent artificial synapses using an implementation of a renewable material of collagen extracted from fish skin with a device structure of Mg/collagen/ITO/PET [110]. The devices exhibited STDP characteristics upon application of a pair of stimuli consisting of a positive pulse (2 V, 10 ms), followed by a negative pulse (−3 V, 10 ms) on the presynaptic and postsynaptic neurons, see figure 22. The brain-inspired electronic synapse also exhibited desirable synaptic characteristics such as analogue switching, potentiation and depression under flat and bent conditions, excitatory postsynaptic current, and paired-pulse facilitation as short-term plasticity. The work demonstrates a significant advance towards efficient analogue hardware implementation using renewable biomaterials.

The development of wearable and implantable memristors provides a promising opportunity to design low-cost and simple-to-make electronic artificial synapses for healthcare and artificial intelligence applications. Recently, wearable neuromorphic computing networks based on stretchable and conformable synapse memristors have been developed by Yang *et al* [111]. The memristors were fabricated on polydimethylsiloxane as the substrate layer by spin coating a solution of Ag nanoparticle-doped thermoplastic polyurethanes (TPU:Ag NPs) as a switching matrix between Au electrodes. The devices showed non-volatile switching properties under relaxed and stretched conditions (up to a

35% strain) as well as demonstrable synaptic functions including potentiation and depression, short-term plasticity (STP) and long-term plasticity (LTP), ‘learning, forgetting and re-learning’ behaviour, and spike-rate-dependent and spike-amplitude-dependent plasticity. Whilst obvious applications include high-performance stretchable and wearable electronics, interestingly, the overall architecture of this system has the potential to conform well to the human brain, which is a highly curved object. Thus, the work could potentially pave the way forward to the development of more complex ‘brain-like’ neuromorphic computing systems.

Besides non-volatile switching (non-temporal or LTP), which is required for memory applications [112], memristors can also show volatile switching (temporal or STP) or temporal dynamic behaviour, which is desirable for neuromorphic and reservoir computing (RC) applications such as speech recognition, classification and time series forecasting [30, 113–116]. Recently, the implementation of a physical RC system has been developed using a 3D-structured, highly ordered mesoporous silica ( $m\text{SiO}_2$ ) based memristor that is fabricated *via* a vacuum-free, low cost and high-speed sol-gel solution processing technique [117]. The 3D-structured  $m\text{SiO}_2$  thin film was sandwiched between TiN and Ag electrodes, TiN/ $m\text{SiO}_2$ /Ag. Although the devices were made on standard silicon substrates, the processes used are still applicable for fabrication on flexible substrates. The fast mobility and diffusivity of  $\text{Ag}^+$  ion species migrating within the 3D porous structures enable the STP behaviour and temporal dynamics. The RC system based on this  $m\text{SiO}_2$  diffusive memristor, demonstrated *in situ* learning capability and a classification accuracy of 100% on a standard machine learning dataset, see figure 23. The devices also showed a bipolar non-volatile switching effect when operated at high compliance currents (CC).

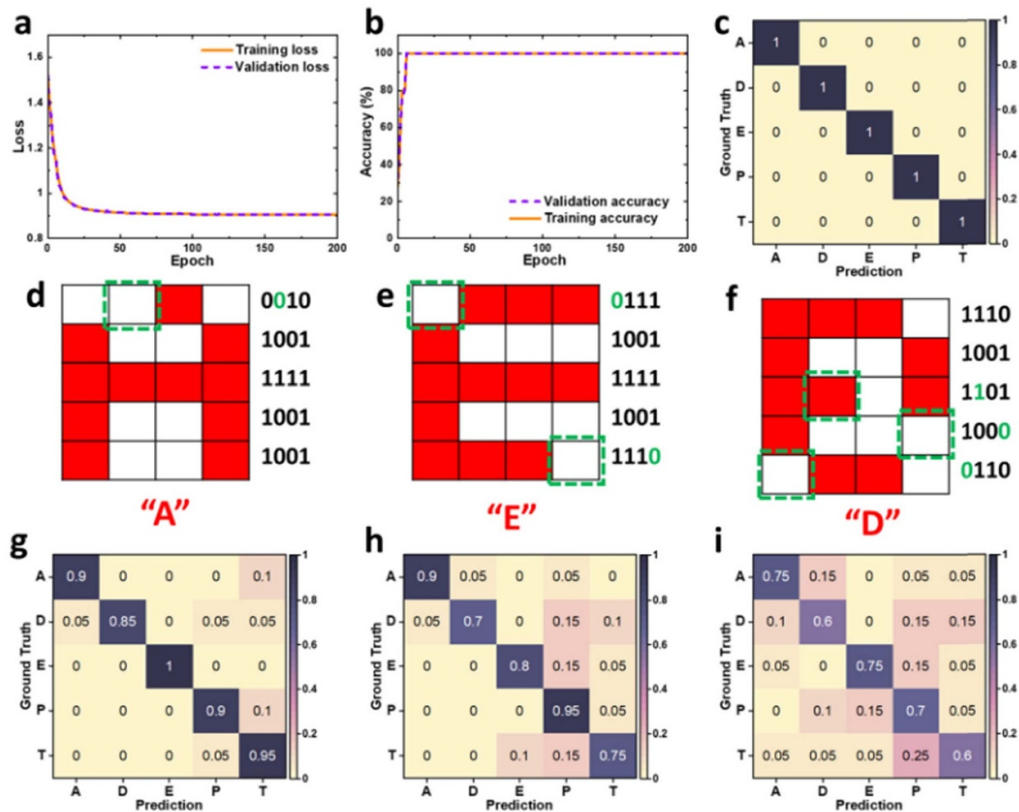


**Figure 23.** Training and performance evaluation of the mSiO<sub>2</sub> memristor-based reservoir computing system. Training and (a) validation loss and (b) validation accuracy as a function of training epochs. (c) Confusion matrix showing the prediction results from the RC system against the ground truth in the test dataset. Examples of letter patterns containing (d) one, (e) two, and (f) three random noises. Confusion matrix showing the prediction results from the RC system against the ground truth for letter patterns in the noisy test dataset containing (g) one, (h) two, and (i) three random noises. Reproduced from [117]. [CC BY 3.0](#).

## 7. Conclusions

Memristors are emerging as attractive candidates for next generation non-volatile memory applications due to their fast-switching speeds, low power consumption, high data storage density, and long cycling endurance and retention times. Whilst potentially filling the role as a universal memory with the possibility to replace conventional semiconductor-based memory technologies (SRAM, DRAM and FLASH), memristors are leading the way in many new and exciting avenues of research in the area of neuromorphic computing, where there is a need to develop new portable, low-energy usage systems by overcoming the problems associated with traditional von Neumann computing architectures such as serial processing and the data-transfer memory bottleneck.

In the last several decades, organic and hybrid (organic-inorganic) composite materials have received enormous attention worldwide because of the wide range of new applications for printed electronics on flexible and lightweight substrates for applications in displays and solar cells, and more recently, new market opportunities in wearable electronics. Printed electronic fabrication techniques offer significant advantages including low cost, fast solution-based processing methods and scalable fabrication of micro and nano- patterning on lightweight, portable, curved, and flexible substrates.

In the field of emerging memory technologies, several exciting papers have recently demonstrated low power consumption, ultrafast switching speeds and impressive performance for neuromorphic computing and artificial intelligence applications based on printed organic and hybrid organic/inorganic memristor devices.

Despite the great deal of attention that has been devoted in the last decade to the field of organic electronics, there is still much remaining progress to be made for the practical use of organic-based memories in commercial applications. In the field of organic memristors there is still device-to-device variability in their manufacture, instability issues because of changes in the ambient conditions (temperature, oxygen gas and moisture) and general problems with fabrication yield and device failure with long-term write/erase cycling. Some of these issues may be resolved with the use of hybrid organic-inorganic composite materials, where there has been significant recent progress with demonstrations of devices with some very excellent performance characteristics that are close to, and in some cases exceed, industry standards. Further advances in this area look promising and should lead to more interest from industry for use in real-world practical applications as well as the development of new applications that have yet to be thought about, let alone discovered.

## Data availability statement

No new data were created or analysed in this study.

## Acknowledgments

This work was partially supported by a Leverhulme Trust Research Project Grant, RPG-2021-115 ‘Ultra-Fast Computer Vision using Highly Parallel Optical Memristor CNN Networks’ awarded to N.K

## ORCID iDs

Ayoub H Jaafar  <https://orcid.org/0000-0001-7305-4542>

Alex Gee  <https://orcid.org/0000-0002-4727-8849>

N T Kemp  <https://orcid.org/0000-0002-1906-4608>

## References

- [1] Moore G E 1965 Cramming more components onto integrated circuits with unit cost *Electronics* **38** 114
- [2] Moore G E 1975 Progress in digital integrated electronics *Int. Electron Devices Meeting (IEEE)* vol 21 pp 11–13
- [3] Theis T N and Philip Wong H S 2017 The end of Moore’s law: a new beginning for information technology *Comput. Sci. Eng.* **19** 41–50
- [4] Williams R S 2017 What’s next? [the end of Moore’s law] *Comput. Sci. Eng.* **19** 7–13
- [5] Gee A, Jaafar A H and Kemp N T 2022 *Memristor Computing Systems* (Springer) pp 219–44
- [6] Ascoli A, Messaris I, Tetzlaff R and Chua L O 2019 CNNs with bistable-like non-volatile memristors: a novel mem-computing paradigm for the IoT era *2018 25th IEEE Int. Conf. on Electronics Circuits and Systems, ICECS* pp 541–4
- [7] Gee A, Jaafar A H, Brachňáková B, Massey J, Marrows C H, Šalitrš I and Kemp N T 2020 Multilevel resistance switching and enhanced spin transition temperature in single- and double-molecule spin crossover nanogap devices *J. Phys. Chem. C* **124** 13393–9
- [8] Chua L O 1971 Memristor-the missing circuit element *IEEE Trans. Circuit Theory* **CT-18** 507–19
- [9] Strukov D B, Snider G S, Stewart D R and Williams R S 2008 The missing memristor found *Nature* **453** 80–83
- [10] Pi S, Li C, Jiang H, Xia W, Xin H, Yang J J and Xia Q 2019 Memristor crossbar arrays with 6-nm half-pitch and 2-nm critical dimension *Nat. Nanotechnol.* **14** 35–39
- [11] Son D, Park D and Kim J 2010 Bistable organic memory device with gold nanoparticles embedded in a conducting poly (N-vinylcarbazole) colloids hybrid *J. Phys. Chem. C* **115** 2341–8
- [12] Kuang Y, Huang R, Tang Y, Ding W, Zhang L and Wang Y 2010 Flexible single-component-polymer resistive memory for ultrafast and highly compatible nonvolatile memory applications *IEEE Electron Device Lett.* **31** 758–60
- [13] Goswami S *et al* 2017 Robust resistive memory devices using solution-processable metal-coordinated azo aromatics *Nat. Mater.* **16** 1216–24
- [14] Son D I, Park D H, Kim J B, Choi J W, Kim T W, Angadi B, Yi Y and Choi W K 2011 Bistable organic memory device with gold nanoparticles embedded in a conducting poly(N-vinylcarbazole) colloids hybrid *J. Phys. Chem. C* **115** 2341–8
- [15] Jaafar A H, Meng L, Zhang T, Guo D, Newbrook D, Zhang W, Reid G, de Groot C H, Bartlett P N and Huang R n.d. Flexible memristor devices using hybrid polymer/electrodeposited GeSbTe nanoscale thin films *ACS Appl. Nano Mater.* **5** 17711–20
- [16] Jaafar A H, Neill M O, Kelly S M, Verrelli E and Kemp N T 2019 Percolation threshold enables optical resistive-memory switching and light-tuneable synaptic learning in segregated nanocomposites *Adv. Electron. Mater.* **5** 1–7
- [17] Kapnopoulos C, Mekeridis E D, Tzounis L, Polyzoidis C, Zachariadis A, Tsimikli S, Gravalidis C, Laskarakis A, Vouroutzis N and Logothetidis S 2016 Fully gravure printed organic photovoltaic modules: a straightforward process with a high potential for large scale production *Sol. Energy Mater. Sol. Cells* **144** 724–31
- [18] Yoon K J, Han J W, Il Moon D, Seol M L, Meyyappan M, Kim H J and Hwang C S 2019 Electrically-generated memristor based on inkjet printed silver nanoparticles *Nanoscale Adv.* **1** 2990–8
- [19] Illarionov G A, Morozova S M, Chrisstop V V, Einarsrud M A and Morozov M I 2020 Memristive TiO<sub>2</sub>: synthesis, technologies, and applications *Front. Chem.* **8** 1–10
- [20] Feng X *et al* 2019 A fully printed flexible MoS<sub>2</sub> memristive artificial synapse with femtojoule switching energy *Adv. Electron. Mater.* **5** 1–9
- [21] Catenacci M J, Flowers P F, Cao C, Andrews J B, Franklin A D and Wiley B J 2017 Fully printed memristors from Cu–SiO<sub>2</sub> core–shell nanowire composites *J. Electron. Mater.* **46** 4596–603
- [22] Gater M, Adawi A M and Kemp N T 2022 Capacitive effects and memristive switching in three terminal multilayered MoS<sub>2</sub> devices *IEEE Int. Symp. on Circuits and Systems (ISCAS) (Austin, TX, USA)* pp 225–9
- [23] Sangwan V K, Lee H S, Bergeron H, Balla I, Beck M E, Chen K S and Hersam M C 2018 Multi-terminal memtransistors from polycrystalline monolayer molybdenum disulfide *Nature* **554** 500–4
- [24] Shima H, Takano F, Muramatsu H, Akinaga H, Tamai Y, Inque I H and Takagi H 2008 Voltage polarity dependent low-power and high-speed resistance switching in CoO resistance random access memory with Ta electrode *Appl. Phys. Lett.* **93** 1–3
- [25] Busby Y, Nau S, Sax S, List-Kratochvil E J W, Novak J, Banerjee R, Schreiber F and Pireaux J J 2015 Direct observation of conductive filament formation in Alq<sub>3</sub> based organic resistive memories *J. Appl. Phys.* **118** 1–6
- [26] Yan P, Li Y, Hui Y J, Zhong S J, Zhou Y X, Xu L, Liu N, Qian H, Sun H J and Miao X S 2015 Conducting mechanisms of forming-free TiW/Cu<sub>2</sub>O/Cu memristive devices *Appl. Phys. Lett.* **107** 083501
- [27] Sun Y, Li Q, Zhu X, Liao C, Wang Y, Li Z, Liu S, Xu H and Wang W 2023 In-sensor reservoir computing based on optoelectronic synapse *Adv. Intell. Syst.* **5** 2200196
- [28] Shabalin A G, Del Valle J, Hua N, Cherukara M J, Holt M V, Schuller I K and Shpyrko O G 2020 Nanoscale imaging and control of volatile and non-volatile resistive switching in VO<sub>2</sub> *Small* **16** 2005439
- [29] Fu Y, Zhou Y, Huang X, Dong B, Zhuge F, Li Y, He Y, Chai Y and Miao X 2022 Reconfigurable synaptic and neuronal functions in a V/VOx/HfWOx/Pt memristor for nonpolar spiking convolutional neural network *Adv. Funct. Mater.* **32** 2111996
- [30] Moon J, Ma W, Shin J H, Cai F, Du C, Lee S H and Lu W D 2019 Temporal data classification and forecasting using a memristor-based reservoir computing system *Nat. Electron.* **2** 480–7

- [31] Takishita Y, Kobayashi M, Hattori K, Matsuda T, Sugisaki S, Nakashima Y and Kimura M 2020 Memristor property of an amorphous Sn-Ga-O thin-film device deposited using mist chemical-vapor-deposition method *AIP Adv.* **10** 035112
- [32] Porro S, Bejtka K, Jasmin A, Fontana M, Milano G, Chiolerio A, Pirri C F and Ricciardi C 2018 A multi-level memristor based on atomic layer deposition of iron oxide *Nanotechnology* **29** 495201
- [33] Gu C and Lee J S 2016 Flexible hybrid organic-inorganic perovskite memory *ACS Nano* **10** 5413–8
- [34] Jaafar A H, Gee A and Kemp N T 2020 Nanorods vs nanoparticles: a comparison study of Au/ZnO-PMMA/Au non-volatile memory devices showing the importance of nanostructure geometry on conduction mechanisms and switching properties *IEEE Trans. Nanotechnol.* **19** 236–46
- [35] Jaafar A H, Lowe C, Gee A and Kemp N T 2023 Optoelectronic switching memory based on ZnO nanoparticle/polymer nanocomposites *ACS Appl. Polym. Mater.* **5** 2367–72
- [36] Gray R J, Jaafar A H, Verrelli E and Kemp N T 2018 Method to reduce the formation of crystallites in ZnO nanorod thin-films grown via ultra-fast microwave heating *Thin Solid Films* **662** 116–22
- [37] Jaafar A H, Gee A, Hamza A O, Eling C J, Bouillard J-S G, Adawi A M and N T Kemp 2020 Evidence of Nanoparticle Migration in Polymeric Hybrid Memristor Devices 2020 *European Conf. on Circuit Theory and Design (ECCTD)* (Sofia, Bulgaria) pp 1–4
- [38] Lanza M *et al* 2021 Standards for the characterization of endurance in resistive switching devices *ACS Nano* **15** 17214–31
- [39] Meng J L *et al* 2021 Flexible boron nitride-based memristor for: in situ digital and analogue neuromorphic computing applications *Mater. Horiz.* **8** 538–46
- [40] Cao Z, Sun B, Zhou G, Mao S S, Zhu S H, Zhang J, Ke C, Zhao Y and Shao J 2023 Memristor-based neural networks: a bridge from device to artificial intelligence *Nanoscale Horiz.* **8** 716–45
- [41] Zhou F *et al* 2019 Optoelectronic resistive random access memory for neuromorphic vision sensors *Nat. Nanotechnol.* **14** 776–82
- [42] Wang J, Shao Y, Li C, Liu B and Yan X 2022 Artificial optoelectronic synapse based on epitaxial Ba<sub>0.6</sub>Sr<sub>0.4</sub>TiO<sub>3</sub> thin films memristor for neuromorphic computing and image recognition *Appl. Phys. Lett.* **121** 262104
- [43] Ye F, Kiani F, Huang Y and Xia Q 2023 Diffusive memristors with uniform and tunable relaxation time for spike generation in event-based pattern recognition *Adv. Mater.* **35** 2204778
- [44] Xia Q *et al* 2009 Memristor-CMOS hybrid integrated circuits for reconfigurable logic *Nano Lett.* **9** 3640–5
- [45] Kim D, Kim S and Kim S 2021 Logic-in-memory application of CMOS compatible silicon nitride memristor *Chaos Solitons Fractals* **153** 111540
- [46] Ma L P, Liu J and Yang Y 2002 Organic electrical bistable devices and rewritable memory cells *Appl. Phys. Lett.* **80** 2997–9
- [47] Ma L, Pyo S, Ouyang J, Xu Q and Yang Y 2003 Nonvolatile electrical bistability of organic/metal-nanocluster/organic system *Appl. Phys. Lett.* **82** 1419–21
- [48] Tondelier D, Lmimouni K, Vuillaume D, Fery C and Haas G 2004 Metal/organic/metal bistable memory devices *Appl. Phys. Lett.* **85** 5763–5
- [49] Nau S, Wolf C, Sax S and List-Kratochvil E J W 2015 Organic non-volatile resistive photo-switches for flexible image detector arrays *Adv. Mater.* **27** 1048–52
- [50] Tu C H, Lai Y S and Kwong D L 2006 Memory effect in the current—voltage characteristic of 8-hydroquinoline aluminum salt films *IEEE Electron Device Lett.* **27** 354–6
- [51] Nau S, Sax S and List-Kratochvil E J W 2014 Unravelling the nature of unipolar resistance switching in organic devices by utilizing the photovoltaic effect *Adv. Mater.* **26** 2508–13
- [52] Tseng R J, Huang J, Ouyang J, Kaner R B and Yang Y 2005 Polyaniline nanofiber/gold nanoparticle nonvolatile memory *Nano Lett.* **5** 1077–80
- [53] Tang W, Shi H Z, Xu G, Ong B S, Popovic Z D, Deng J C, Zhao J and Rao G H 2005 Memory effect and negative differential resistance by electrode- induced two-dimensional single- electron tunneling in molecular and organic electronic devices *Adv. Mater.* **17** 2307–11
- [54] Paul F and Paul S 2022 To be or not to be—review of electrical bistability mechanisms in polymer memory devices *Small* **18** 2106442
- [55] Kaiser A B, Liu C-J, Gilberd P W, Chapman B, Kemp N T, Wessling B, Partridge A C, Smith W T and Shapiro J S 1997 Comparison of electronic transport in polyaniline blends, polyaniline and polypyrrole *Synth. Met.* **84** 699–70
- [56] Lee J-K, Cho J M, Shin W S, Moon S J, Kemp N T, Zhang H and Lamb R 2008 The stability of PEDOT:PSS films monitored by electron spin resonance *J. Korean Phys. Soc.* **52** 621–6
- [57] Jabarullah N H, Verrelli E, Mauldin C, Navarro L A, Golden J, Madianos L, Tsoukalas D and Kemp N T 2014 Novel conducting polymer current limiting devices for low cost surge protection applications *J. Appl. Phys.* **116** 164501
- [58] Waser R, Dittmann R, Staikov C and Szot K 2009 Redox-based resistive switching memories nanoionic mechanisms, prospects, and challenges *Adv. Mater.* **21** 2632–63
- [59] Peng S *et al* 2012 Mechanism for resistive switching in chalcogenide-based electrochemical metallization memory *Appl. Phys. Lett.* **100** 072101
- [60] Valov I, Linn E, Tappertzhofen S, Schmelzer S, Van Den Hurk J, Lentz F and Waser R 2013 Nanobatteries in redox-based resistive switches require extension of memristor theory *Nat. Commun.* **4** 1771–9
- [61] Cho B, Yun J M, Song S, Ji Y, Kim D Y and Lee T 2011 Direct observation of Ag filamentary paths in organic resistive memory devices *Adv. Funct. Mater.* **21** 3976–81
- [62] Paul S, Pearson C, Molloy A, Cousins M A, Green M, Kolliopoulou S, Dimitrakis P, Normand P, Tsoukalas D and Petty M C 2003 Langmuir-Blodgett film deposition of metallic nanoparticles and their application to electronic memory structures *Nano Lett.* **3** 533–6
- [63] Ouyang J, Chu C-W, Szmada C R, Ma L and Yang Y 2004 Programmable polymer thin film and non-volatile memory device *Nat. Mater.* **3** 918–22
- [64] Qi M, Cao S, Yang L, You Q, Shi L and Wu Z 2020 Uniform multilevel switching of graphene oxide-based RRAM achieved by embedding with gold nanoparticles for image pattern recognition *Appl. Phys. Lett.* **116** 1–5
- [65] Mukherjee B and Mukherjee M 2009 Nonvolatile memory device based on Ag nanoparticle: characteristics improvement *Appl. Phys. Lett.* **94** 173510
- [66] Pei Y, Yan L, Wu Z, Lu J, Zhao J, Chen J, Liu Q and Yan X 2021 Artificial visual perception nervous system based on low-dimensional material photoelectric memristors *ACS Nano* **15** 17319–26
- [67] Yan X *et al* 2019 Self-assembled networked PbS distribution quantum dots for resistive switching and artificial synapse performance boost of memristors *Adv. Mater.* **31** 1805284
- [68] Bera J, Betal A, Sharma A, Shankar U, Rath A K and Sahu S 2022 CdSe quantum dot-based nanocomposites for

- ultralow-power memristors *ACS Appl. Nano Mater.* **5** 8502–10
- [69] Chen Z *et al* 2020 Broadband photoelectric tunable quantum dot based resistive random access memory *J. Mater. Chem. C* **8** 2178–85
- [70] Liu G, Zhuang X, Chen Y, Zhang B, Zhu J, Zhu C X, Neoh K G and Kang E T 2009 Bistable electrical switching and electronic memory effect in a solution-processable graphene oxide-donor polymer complex *Appl. Phys. Lett.* **95** 2007–10
- [71] Nagareddy V K, Barnes M D, Zipoli F, Lai K T, Alexeev A M, Craciun M F and Wright C D 2017 Multilevel ultrafast flexible nanoscale nonvolatile hybrid graphene oxide-titanium oxide memories *ACS Nano* **11** 3010–21
- [72] Thakre A, Borkar H, Singh B P and Kumar A 2015 Electroforming free high resistance resistive switching of graphene oxide modified polar-PVDF *RSC Adv.* **5** 57406–13
- [73] Khurana G, Misra P, Kumar N, Kooriyattil S, Scott J F and Katiyar R S 2016 Enhanced resistive switching in forming-free graphene oxide films embedded with gold nanoparticles deposited by electrophoresis *Nanotechnology* **27** 1–7
- [74] Anoop G, Panwar V, Kim T Y and Jo J Y 2017 Resistive switching in ZnO nanorods/graphene oxide hybrid multilayer structures *Adv. Electron. Mater.* **3** 1–9
- [75] Son D I, Kim T W, Shim J H, Jung J H, Lee D U, Lee J M, U Park W and Choi W K 2010 Flexible organic bistable devices based on graphene embedded in an insulating poly(methyl methacrylate) polymer layer *Nano Lett.* **10** 2441–7
- [76] Zhuang B X, Chen Y, Liu G, Li P, Zhu C, Kang E, Neoh K, Zhang B, Zhu J and Li Y 2010 Conjugated-polymer-functionalized graphene oxide: synthesis and nonvolatile rewritable memory effect *Adv. Mater.* **22** 1–5
- [77] Jaafar A H, Gray R J, Verrelli E, O'Neill M, Kelly S M and Kemp N T 2017 Reversible optical switching memristors with tunable STDP synaptic plasticity: a route to hierarchical control in artificial intelligent systems *Nanoscale* **9** 17091–8
- [78] Jaafar A H, Lowe C, Gee A and Kemp N T 2023 Optoelectronic switching memory based on ZnO Nanoparticle/Polymer nanocomposites *ACS Appl. Polym. Mater.* **5** 2367–73
- [79] Jaafar A H, Al Chawa M M, Cheng F, Kelly S M, Picos R, Tetzlaff R and Kemp N T 2021 Polymer/TiO<sub>2</sub> nanorod nanocomposite optical memristor device *J. Phys. Chem. C* **125** 14965–73
- [80] Liu G, Ling Q, Yeow E, Teo H, Zhu C, Chan D S and Neoh K 2009 Electrical conductance tuning and bistable switching in Poly(N-vinylcarbazole)-carbon nanotube composite films *ACS Nano* **3** 1929–37
- [81] Sharma B K and Ahn J H 2016 Flexible and stretchable oxide electronics *Adv. Electron. Mater.* **2** 1–17
- [82] Biggs J, Myers J, Kufel J, Ozer E, Craske S, Sou A, Ramsdale C, Williamson K, Price R and White S 2021 A natively flexible 32-bit Arm microprocessor *Nature* **595** 532–6
- [83] Han S T, Zhou Y and Roy V A L 2013 Towards the development of flexible non-volatile memories *Adv. Mater.* **25** 5425–49
- [84] Yan Z, Guo Y, Zhang G and Liu J M 2011 High-performance programmable memory devices based on Co-doped BaTiO<sub>3</sub> *Adv. Mater.* **23** 1351–5
- [85] Lee M J *et al* 2013 A plasma-treated chalcogenide switch device for stackable scalable 3d nanoscale memory *Nat. Commun.* **4** 2629
- [86] Yan X *et al* 2019 Robust Ag/ZrO<sub>2</sub>/WS<sub>2</sub>/Pt memristor for neuromorphic computing *ACS Appl. Mater. Interfaces* **11** 48029–38
- [87] Choi B J *et al* 2005 Resistive switching mechanism of TiO<sub>2</sub> thin films grown by atomic-layer deposition *J. Appl. Phys.* **98** 033715
- [88] Blayo A and Pineaux B 2005 *Printing Processes and Their Potential for RFID Printing*
- [89] Sung D, de La Fuente Vornbrock A and Subramanian V 2010 Scaling and optimization of gravure-printed silver nanoparticle lines for printed electronics *IEEE Trans. Compon. Packag. Technol.* **33** 105–14
- [90] Lee T M, Lee S H, Noh J H, Kim D S and Chun S 2010 The effect of shear force on ink transfer in gravure offset printing *J. Micromech. Microeng.* **20** 125026
- [91] Khan S, Lorenzelli L and Dahiya R S 2015 Technologies for printing sensors and electronics over large flexible substrates: a review *IEEE Sens. J.* **15** 3164–85
- [92] Calvert P 2001 Inkjet printing for materials and devices *Chem. Mater.* **13** 3299–305
- [93] de Gans B J, Duineveld P C and Schubert U S 2004 Inkjet printing of polymers: state of the art and future developments *Adv. Mater.* **16** 203–13
- [94] Andò B and Baglio S 2011 Inkjet-printed sensors: a useful approach for low cost, rapid prototyping [instrumentation notes] *IEEE Instrum. Meas. Mag.* **14** 36–40
- [95] Christenson K K, Paulsen J A, Renn M J, McDonald K, Bourassa J and 2011 Direct Printing of Circuit Boards Using Aerosol Jet® *NIP & Digital Fabrication Conf.* vol 27 pp 433–6
- [96] Ribierre J C, Aoyama T, Muto T and André P 2011 Hybrid organic-inorganic liquid bistable memory devices *Org. Electron.* **12** 1800–5
- [97] Jaafar A H and Kemp N T 2019 Wavelength dependent light tunable resistive switching graphene oxide nonvolatile memory devices *Carbon* **153** 81–88
- [98] Xu Y, Wang H, Ye D, Yang R, Huang Y and Miao X 2022 Electrohydrodynamically printed flexible organic memristor for leaky integrate and fire neuron *IEEE Electron Device Lett.* **43** 116–9
- [99] Siddiqui G U, Rehman M M and Choi K H 2016 Enhanced resistive switching in all-printed, hybrid and flexible memory device based on perovskite ZnSnO<sub>3</sub> via PVOH polymer *Polymer* **100** 102–10
- [100] Lien D H, Kao Z K, Huang T H, Liao Y C, Lee S C and He J H 2014 All-printed paper memory *ACS Nano* **8** 7613–9
- [101] Bessonov A A, Kirikova M N, Petukhov D I, Allen M, Ryhänen T and Bailey M J A 2015 Layered memristive and memcapacitive switches for printable electronics *Nat. Mater.* **14** 199–204
- [102] Zhu K *et al* 2023 Inkjet-printed h-BN memristors for hardware security *Nanoscale* **15** 9985–92
- [103] Rehman M M, Yang B S, Yang Y J, Karimov K S and Choi K H 2017 Effect of device structure on the resistive switching characteristics of organic polymers fabricated through all printed technology *Curr. Appl. Phys.* **17** 533–40
- [104] Mao J Y, Zhou L, Zhu X, Zhou Y and Han S T 2019 Photonic memristor for future computing: a perspective *Adv. Opt. Mater.* **7** 1900766
- [105] Lyapunov N *et al* 2022 A bifunctional memristor enables multiple neuromorphic computing applications *Adv. Electron. Mater.* **8** 2101235

- [106] Hebb D O 1949 *The Organization of Behavior: A Neuropsychological Theory* (Wiley, Chapman and Hall) p 335
- [107] Park Y and Lee J S 2017 Artificial synapses with short- and long-term memory for spiking neural networks based on renewable materials *ACS Nano* **11** 8962–9
- [108] Markram H, Lubke J, Frotscher M and Sakmann B 1997 Regulation of synaptic efficacy by coincidence of postsynaptic APs and EPSPs *Science* **275** 213–5
- [109] Šuch O, Klimo M, Kemp N T and Škvarek O 2018 Passive memristor synaptic circuits with multiple timing dependent plasticity mechanisms *AEU-Int. J. Electron. Commun.* **96** 252–9
- [110] Raeis-Hosseini N, Park Y and Lee J S 2018 Flexible artificial synaptic devices based on collagen from fish protein with spike-timing-dependent plasticity *Adv. Funct. Mater.* **28** 1800553
- [111] Yang M, Zhao X, Tang Q, Cui N, Wang Z, Tong Y and Liu Y 2018 Stretchable and conformable synapse memristors for wearable and implantable electronics *Nanoscale* **10** 18135–44
- [112] Feng Y, Gao X, Zhong Y-N, Wu J-L, Xu J-L and Wang S-D 2019 Solution-processed polymer thin-film memristors with an electrochromic feature and frequency-dependent synaptic plasticity *Adv. Intell. Syst.* **1** 1900022
- [113] Midya R, Wang Z, Asapu S, Zhang X, Rao M, Song W, Zhuo Y, Upadhyay N, Xia Q and Yang J J 2019 Reservoir computing using diffusive memristors *Adv. Intell. Syst.* **1** 1900084
- [114] Du C, Cai F, Zidan M A, Ma W, Lee S H and Lu W D 2017 Reservoir computing using dynamic memristors for temporal information processing *Nat. Commun.* **8** 2204
- [115] Yang J, Cho H, Ryu H, Ismail M, Mahata C and Kim S 2021 Tunable synaptic characteristics of a Ti/TiO<sub>2</sub>/Si memory device for reservoir computing *ACS Appl. Mater. Interfaces* **13** 33244–52
- [116] Milano G, Pedretti G, Montano K, Ricci S, Hashemkhani S, Boarino L, Ielmini D and Ricciardi C 2022 In materia reservoir computing with a fully memristive architecture based on self-organizing nanowire networks *Nat. Mater.* **21** 195–202
- [117] Jaafar A H, Shao L, Dai P, Zhang T, Han Y, Beanland R, Kemp N T, Bartlett P N, Hector A L and Huang R 2022 3D-structured mesoporous silica memristors for neuromorphic switching and reservoir computing *Nanoscale* **14** 17170–81